Retrieving Particulate Matter Concentrations over the Contiguous United States Using CALIOP Observations

Travis D. Toth[1], Jianglong Zhang[2], Mark A. Vaughan[1], Jeffrey S. Reid[3], and James R. Campbell[3]

[1]NASA Langley Research Center, Hampton, VA
[2]University of North Dakota, Grand Forks, ND
[3]Naval Research Laboratory, Monterey, CA

Submitted to:

Atmospheric Environment

(2021)

Keywords: CALIOP; LIDAR; Aerosols; $PM_{2.5}$; Air quality; Aerosol trends

Corresponding Author: travis.d.toth@nasa.gov

Abstract

Using twelve years (2007-2018) of NASA Cloud-Aerosol Lidar with Orthogonal Polarization (CALIOP) near-surface 532 nm aerosol extinction retrievals, multi-year mean and trends of particulate matter (PM) concentrations are derived over the contiguous United States (CONUS). Different from past studies that use column integrated aerosol optical thickness, here only near-surface CALIOP aerosol extinction is used for deriving near-surface PM with aerodynamic diameters less than 2.5 μm ($PM_{2.5}$) concentrations using an innovative, bulk-mass-modeling-based method. Compared against ground based $PM_{2.5}$ measurements from the U.S. Environmental Protection Agency (EPA), an encouraging relationship between CALIOP-derived $PM_{2.5}$ and EPA-observed $PM_{2.5}$ (Deming slope = 0.89; RMSE = 3.42 $\mu g/m^3$; mean bias = -1.00 $\mu g/m^3$) is found using combined daytime/nighttime CALIOP data. Also, comparable trends in $PM_{2.5}$ concentrations from the EPA and daytime and nighttime CALIOP data are found for most of the eastern CONUS and imply that air quality is generally improving over this region for the study period. Over the western CONUS, a seasonal analysis reveals that $PM_{2.5}$ trends are positive during the more active wildfire season (June through November) but negative for other months. This study suggests that lidar data show promise in their use for obtaining $PM_{2.5}$ estimates and provides motivation to further explore aerosol extinction-based PM concentration retrievals in anticipation of future space-based lidar missions.

1 Introduction

Aerosol particles, especially particulate matter (PM) with aerodynamic diameters smaller than 2.5 μm ($PM_{2.5}$), contribute to air pollution and negatively impact human health (e.g., Schwartz et al., 1996; Pope et al., 2002; Xing et al., 2016). As such, the United States (U.S.) Environmental Protection Agency (EPA) continually monitors $PM_{2.5}$ concentrations across the country through a ground-based network of *in situ* instruments to support air quality forecasting and decision making for environment-related policies (e.g., Padgett and Richmond, 1983; Federal Register, 1997). However, while the U.S., as well as members of the European Union, have extensive monitoring networks with freely available data, measurements are more limited over many areas of the world. In response, researchers have investigated the use of aerosol optical thickness (AOT) derived from space-based passive remote sensing instruments for $PM_{2.5}$ applications (e.g., Chu et al., 2003; Wang and Christopher, 2003; Van Donkelaar et al., 2006; Lee et al., 2012; Xie et al., 2015). These past efforts have been primarily based upon correlative relationships between EPA $PM_{2.5}$ and satellite-based AOT estimates (e.g., Hoff and Christopher, 2009 and references therein), with some studies leveraging chemical transport models in an attempt to improve the $PM_{2.5}$/AOT relationship (e.g., Liu et al., 2004; Van Donkelaar et al., 2016).

The clear advantage of the passive remote sensor AOT approach to estimating $PM_{2.5}$ comes from the large spatial and temporal coverages that satellites provide. However, $PM_{2.5}$ concentrations are surface-based measurements in units of micrograms per cubic meter, whereas AOT is a unitless column-integrated property that measures the amount of attenuation of solar energy due to aerosols through the full atmospheric column. Thus, for elevated aerosol plumes above the planetary boundary layer (PBL) and near-ground surface layer effects, $PM_{2.5}$ and AOT can be uncorrelated (e.g., Toth et al., 2014; Reid et al., 2017). Also, while AOT provides a single,

column-integrated estimate of aerosol loading, vertical variations in particle size and hygroscopic growth within a column can be large and are often non-uniformly distributed. Therefore, AOT is not necessarily a reliable proxy for surface $PM_{2.5}$ concentrations in many cases (e.g., Hand and Malm, 2007; Toth et al., 2014; Kaku et al., 2018).

An alternate approach to using radiometric proxy estimates derived from passive remote sensors is to directly derive $PM_{2.5}$ concentrations using aerosol extinction profiled near the Earth's surface using range-resolved measurements from space-based lidars. The advantage here is that discrete near-surface extinction coefficients can more accurately capture aerosol optical properties at the surface than an integrated parameter such as AOT. In a recent proof-of-concept study, Toth et al. (2019) describe a bulk-mass-modeling method to directly retrieve $PM_{2.5}$ using near-surface Cloud-Aerosol Lidar with Orthogonal Polarization (CALIOP) observations over the contiguous United States (CONUS) for a two-year (2008-2009) period. In this algorithm, $PM_{2.5}$ concentration or aerosol mass concentration is derived by dividing the CALIOP retrieved near-surface extinction coefficient by the product of the aerosol mass extinction efficiency (e.g., Liou, 2002; Chow et al., 2006; Hand and Malm, 2007), the hygroscopic growth of particles, and inverse of the $PM_{2.5}$ to PM_{10} (particulate matter with aerodynamic diameters smaller than 10 μm) conversion ratio. The analyses resulted in R^2 values between EPA $PM_{2.5}$ and CALIOP-derived $PM_{2.5}$ ranging from ~0.2 for daytime CALIOP observations to ~0.5 for nighttime observations.

We now examine the feasibility of applying the algorithm described in Toth et al. (2019) to nearly the entire data record of CALIOP (2007-2018) and study the long-term means and trends of the derived $PM_{2.5}$ concentration over the CONUS. We restrict the analysis to the CONUS to maximize our opportunities for comparisons with the very large number of well-validated ground-based $PM_{2.5}$ measurements acquired by the EPA. We investigate the regional variability of EPA

and CALIOP-based $PM_{2.5}$ concentrations over the CONUS and describe sensitivity studies of assumed mixed layer height (defined as those near-surface CALIOP range bins used for deriving $PM_{2.5}$) and. Because traditional AOT/$PM_{2.5}$ studies frequently use full column AOT as a proxy for near-surface aerosol extinction (e.g., Hoff and Christopher, 2009), in this work we report the mean state and trends in the contribution of near-surface aerosols to those of the total atmospheric column. We focus on the following research questions:

1. How consistent is the Toth et al. (2019) algorithm when extended over twelve years of CALIOP data?
2. Do any trends in CALIOP-derived $PM_{2.5}$ over the CONUS appear in the data, and how do they compare with those from EPA?
3. Are there regional and/or seasonal differences in the mean state and trend of EPA versus CALIOP-derived $PM_{2.5}$ concentrations throughout the CONUS during the study period?
4. How sensitive are the EPA/CALIOP $PM_{2.5}$ correlations to the assumed mixed layer height?
5. How does the fraction of near-surface AOT to column AOT vary over the study time period?

The primary goal of this research is to address the 2017 NASA Decadal Survey that prioritizes the need for an increased understanding of air pollution distribution and its trends (National Academies, 2018) and lays the foundation for the future characterization of air pollution from the next lidars in space (e.g., NASA Atmosphere Observing System; Stephens et al., 2021). The $PM_{2.5}$ analyses provided in this paper have the potential for use in air quality research, applications, and model validation, helping to quantify $PM_{2.5}$ concentrations over areas with few

to no surface stations, and setting the stage for the development of a more robust CALIOP-based $PM_{2.5}$ product with possible implementation on a global scale.

2 Data, Methods, and Algorithm

2.1 EPA data

The EPA operates an extensive network of ground stations across the country that routinely monitor atmospheric components responsible for degrading regional air quality, including criteria gases (ozone, SO_2, CO, and NO_2) and particulate matter ($PM_{2.5}$ and PM_{10}), providing data at daily and hourly resolutions (U.S. EPA, 2020). $PM_{2.5}$ measurements are acquired through a variety of instruments that adhere to Federal Reference Method (FRM; gravimetric analysis) and Federal Equivalent Method (FEM; taper element oscillating microbalance [TEOM] and beta gauge analyses) regulations (Federal Register, 1997; Noble et al., 2001; Greenstone, 2002). In this study, twelve years (2007-2018) of Daily $PM_{2.5}$ Local Conditions data (parameter code 88101) from EPA stations are used for analysis, obtained from the EPA Air Quality System (AQS). This dataset is comprised mostly of 24-hour filter-based (i.e., gravimetric) measurements, but also includes an average of hourly TEOM or beta gauge measurements over a 24-hour period for some stations. Uncertainties in EPA $PM_{2.5}$ data are instrument/method dependent, as summarized in Toth et al. (2019), and explanations of $PM_{2.5}$ uncertainties in a greater level of detail can be found in other studies (e.g., Spagnolo, 1989; Chung et al., 2001; Patashnick et al., 2001; Eatough et al, 2003; Kiss et al., 2017).

2.2 CALIPSO data

Operational since 2006, CALIOP is a dual-wavelength (532 nm and 1064 nm) polarization-sensitive (at 532 nm) elastic backscatter lidar flying aboard the Cloud-Aerosol Lidar and Infrared Pathfinder Satellite Observations (CALIPSO) satellite, providing a vertically-resolved perspective of aerosols and clouds in the atmosphere to the limit of signal attenuation (Winker et al., 2010). The range-resolved aerosol measurements made by CALIOP have been applied for air quality studies, including those involving $PM_{2.5}$ (e.g., Toth et al., 2014; 2019; Bin et al., 2021; Fang et al., 2021) and detection/movement of pollution episodes (e.g., Tao et al., 2012; Kar et al., 2015; Chen et al., 2018; Yin et al., 2021). Initially a member of the "A-Train" satellite constellation (Stephens et al., 2018), CALIPSO joined CloudSat in its orbit in late 2018 to form the "C-Train" satellite constellation (flying ~16.5 km below "A-Train"; e.g., Yeom et al., 2020).

In this study, twelve years (2007-2018) of 532 nm extinction coefficient from the V4.10 CALIOP Level 2 5 km aerosol profile (L2_05kmAPro) product are analyzed over the CONUS during both daytime and nighttime conditions, respectively. The ending year of 2018 was chosen due to CALIPSO's new orbit in the "C-Train" after that time and the desire to have consistent sampling for the trend analysis. The method used here for processing CALIPSO aerosol data is consistent with several previous papers, all of which provide detailed explanations (Toth et al., 2014; 2016; 2019). In a general sense, the CALIPSO data are first subject to rigorous quality assurance (QA) and cloud screening procedures, similar to those described in Kittaka et al. (2011), Campbell et al. (2012), and Winker et al. (2013), through the use of parameters from the L2_05kmAPro and CALIOP Level 2 5 km aerosol layer (L2_05kmALay) products. The specific QA parameters and thresholds used in this study are outlined in Toth et al. (2019). The aerosol profiles are then linearly re-gridded from 60 m vertical resolution (above mean sea level; AMSL) to 100 m bins, referenced to the local surface (above ground level; AGL). The means of aerosol

extinction are then computed for the 100-1000 m AGL altitude range, and this is defined as near-surface aerosol extinction for this study. The lowest 100 m bin is not considered due to potential surface contamination in aerosol extinction (e.g., Kim et al., 2017; Toth et al., 2019), but sensitivity studies concerning this topic are explored in Sect. 3.3. For later validation purposes, CALIOP data are spatially (within 100 km) and temporally (same day) collocated with data from the EPA (consistent with Toth et al., 2019).

2.3 Methods and Algorithm

As described in Toth et al. (2019), the algorithm to derive PM mass concentration ($\mu g/m^3$) is based on the normalization of the 532 nm extinction coefficient (km^{-1}) by the mass extinction (scattering + absorption) efficiency (m^2/g; Liou, 2002; Chow et al., 2006), written as

$$C_m = \frac{\sigma \times 1000}{(\alpha_{scat} \times f_{rh} + \alpha_{abs})}, \quad (1)$$

where is σ is the CALIOP-derived mean near-surface (100-1000 m AGL) aerosol extinction coefficient, α_{scat} and α_{abs} are the dry mass scattering and absorption efficiencies, respectively, f_{rh} is the hygroscopic growth factor, and C_m is the PM mass concentration. Pollution particle composition is assumed to be essentially uniform over all of the CONUS, and hence the corresponding α_{scat} and α_{abs} values used are 3.40 m^2/g and 0.37 m^2/g, respectively. These values were obtained from the Optical Properties of Aerosols and Clouds (OPAC) model (Hess et al., 1998) and are consistent with previous studies (e.g., Hand and Malm, 2007; Kaku et al., 2018). We recognize that the assumption of one aerosol type over the entire CONUS is a significant simplification. A future study is planned to fully investigate the effect of different aerosol types

(and subsequent mass scattering/absorption efficiencies) on extinction-based retrievals of $PM_{2.5}$ concentrations, similar in principle to the analysis of Omar et al. (2005) that develops an optical model for six modular global aerosol types that served as a predicate to the original species distinguished by CALIOP algorithms (Omar et al., 2009).

Also, note that in order to focus on fine mode aerosols, we exclude extinction range bins classified as pure dust (which exhibit a_{scat} values ~0.5-0.7 m^2/g; e.g., Malm and Hand, 2007) by the CALIPSO aerosol typing algorithms. We acknowledge, however, that dust is not coarse mode alone (e.g., Omar et al., 2005), and some fine mode dust will be present in the EPA-observed $PM_{2.5}$ concentrations. This is particularly true over parts of the western CONUS, where dust aerosols are generally more prevalent compared to other regions in the CONUS (e.g., Omar et al., 2009). Thus, our choice to remove CALIOP-classified dust profiles may impact the performance of our $PM_{2.5}$ derivations when comparing to ground station data, and also lowers the number of CALIPSO points available for analysis (e.g., especially over the western CONUS, as discussed further in Sect. 3). The implications of removing dust will be fully explored in a future study in CALIOP-derived $PM_{2.5}$ concentrations as a function of aerosol type.

Furthermore, the hygroscopic growth factor is a necessary component of Eq. (1) because *in situ* $PM_{2.5}$ are dry mass measurements, but extinction retrievals consider aerosol humidification effects. This factor is computed from Modern-Era Retrospective analysis for Research and Applications Version 2 (MERRA-2) relative humidity (RH) profiles included in the CALIPSO datasets using the approach by Hänel (1976), as

$$f_{rh} \quad \left(\frac{1 \quad RH}{1 \quad RH_{ref}}\right)^{\Gamma}, \qquad (2)$$

where RH_{ref} is the reference RH (30% for this analysis; Lynch et al., 2016) and Γ is a unitless light scattering hygroscopicity fit parameter (0.63 for this study, assuming sulfate aerosol; e.g., Toth et al., 2019). A $PM_{2.5}$ to PM_{10} ratio (ϕ) is also considered in the $PM_{2.5}$ derivation algorithm, as extinction-derived PM mass concentration is for all particle sizes and $PM_{2.5}$ represents only those particles with diameters smaller than 2.5 μm. A ϕ value of 0.6 was used here, as reported in a past study (Kaku et al., 2018). Equation 1 can thus be rewritten as:

$$C_{m2.5} = \frac{\sigma \times \phi \times 1000}{(\alpha_{scat} \times f_{rh} + \alpha_{abs})} \quad , \qquad (3)$$

where $C_{m2.5}$ is CALIOP-derived $PM_{2.5}$ concentration ($\mu g/m^3$).

3 Results and Discussion

3.1 Spatial and temporal patterns of $PM_{2.5}$ from CALIOP and ground-based observations

The yearly variation in $PM_{2.5}$ concentrations from EPA *in situ* instruments across the CONUS was analyzed. A map of the EPA sites with available $PM_{2.5}$ daily data from 2007 to 2018, including our arbitrary boundaries of four geographic regions within the CONUS, provided for context of a subsequent regional analysis, is shown in Fig. 1. Figure 2 shows the 3º x 3º yearly-mean $PM_{2.5}$ concentrations at EPA ground stations from 2007 to 2018, computed from the daily $PM_{2.5}$ measurements. A minimum of fifty observations per 3º x 3º grid box was required in order to be included in the analysis. Consistent spatial patterns of $PM_{2.5}$ generally emerge regardless of year, with higher concentrations in both the eastern and western CONUS (especially California), and lower concentrations across the central CONUS. This pattern is consistent with other studies

255 (e.g., Hand et al., 2013; Ford et al., 2018; Gantt et al., 2020). In terms of yearly variation, $PM_{2.5}$
256 in the eastern CONUS is higher early in the study period and decreases in the later years, likely
257 demonstrating the effects of air quality regulation (e.g., Tosca et al., 2017; Hand et al., 2020). For
258 other CONUS regions, it is more difficult to discern any significant yearly variation, as the plots
259 of Fig. 2 suggest little change in $PM_{2.5}$ concentrations over the study period. A detailed trend study
260 is developed in Sect. 3.2.

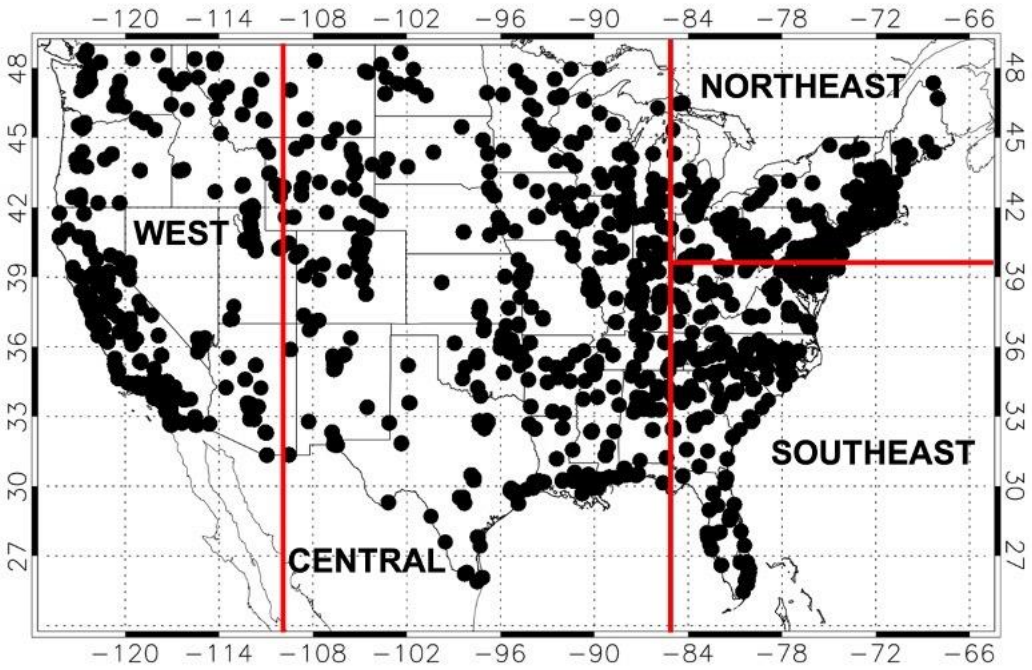

Figure 1. Map of the CONUS showing the locations of U.S. EPA stations that report daily $PM_{2.5}$ concentration observations (Parameter Code: 88101) during the study time period (2007-2018). The red lines delineate the boundaries of four regions: West (≤ -110° longitude), Central (> -110° and ≤ -85° longitude), Northeast (> -85° longitude and ≥ 40° latitude), and Southeast (> -85° longitude and < 40° latitude).

261

262

263

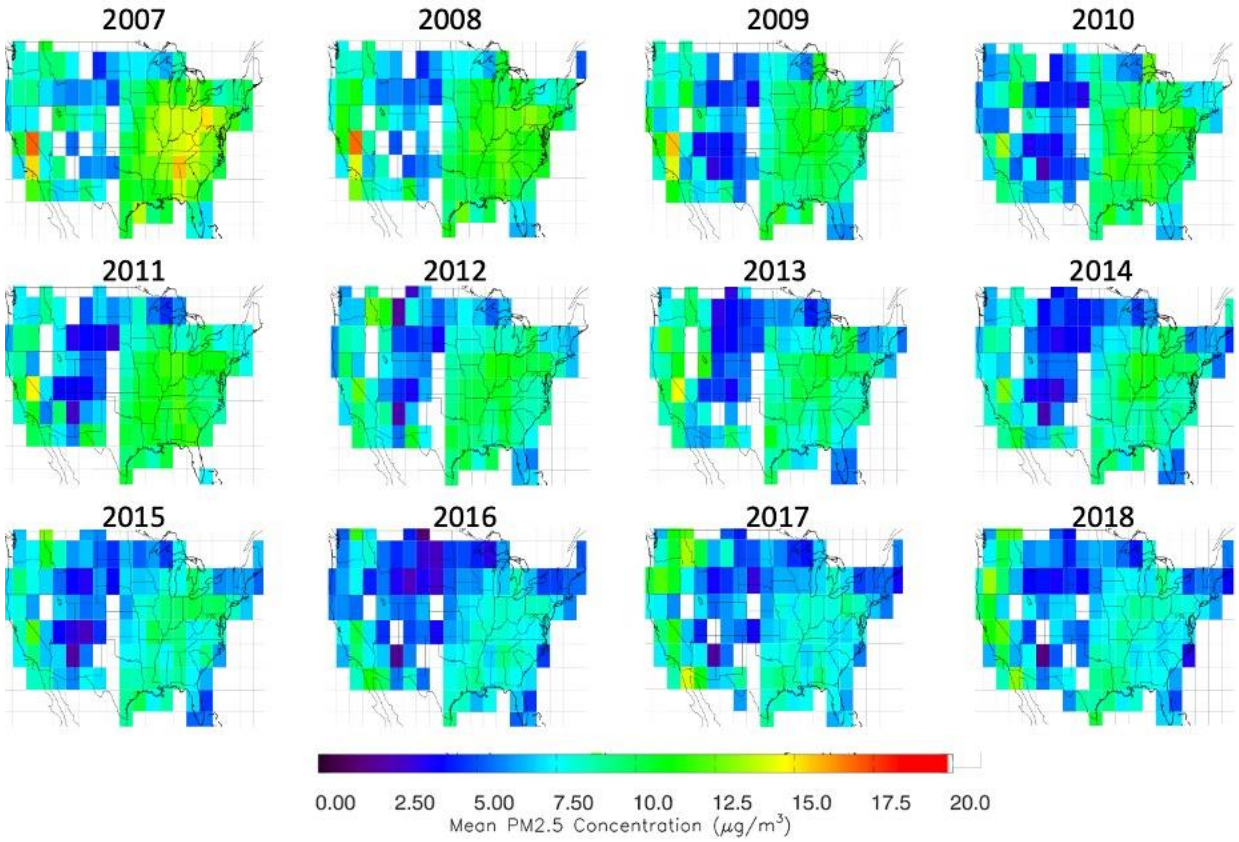

Figure 2. For 2007 to 2018, yearly mean $PM_{2.5}$ concentrations, computed from daily measurements and gridded at 3º x 3º latitude/longitude resolution, from EPA sites across the CONUS.

We used Eqn. 3 to derive $PM_{2.5}$ from CALIOP near-surface aerosol extinction (100-1000 m AGL). Using daytime CALIOP measurements (i.e., the near 1330 UTC equator local-time half-orbital granule), 3º x 3º yearly mean $PM_{2.5}$ concentrations are shown in Fig. 3 for the CONUS over the study period. Note that we require a minimum of fifty points per 3º x 3º grid box, and these yearly means include 100-1000 m aerosol extinction points that are equal to zero from lack of detection sensitivity (e.g., Toth et al., 2018). While there is some noise in the spatial distribution, a broad pattern is observed: higher $PM_{2.5}$ in the eastern CONUS, lower $PM_{2.5}$ in the central CONUS, and some areas, like California and Idaho, in the western CONUS with higher $PM_{2.5}$ concentrations.

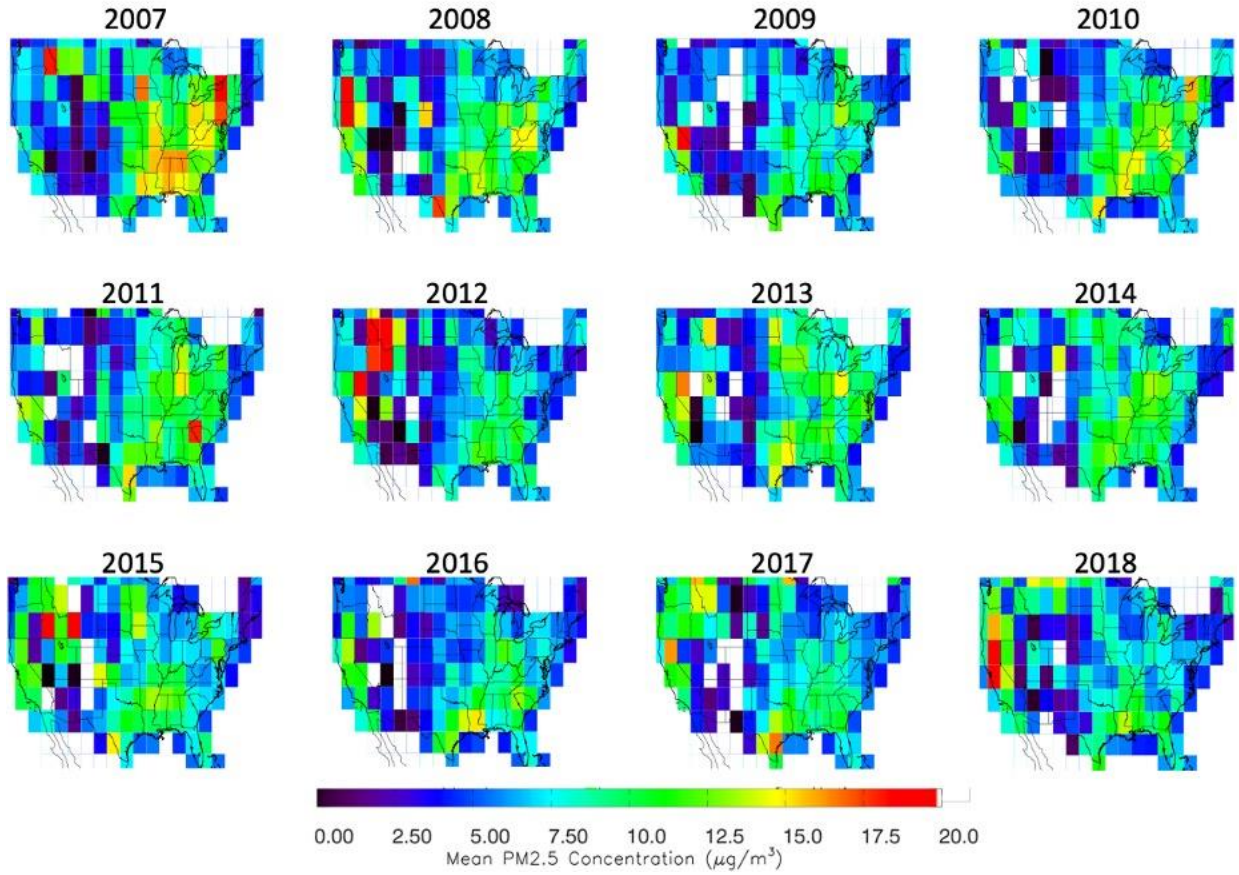

Figure 3. For 2007 to 2018 over the CONUS, 3º x 3º yearly mean $PM_{2.5}$ concentrations derived from daytime CALIOP near-surface (100-1000 m AGL) aerosol extinction.

Our investigations into these enhanced levels of $PM_{2.5}$ concentrations in Idaho in 2012, for example, showed they are due to increased wildfire activity in August and September 2012 (e.g., Mallia et al., 2014) that increases the 2012 yearly mean $PM_{2.5}$ for this area. Also, over the western CONUS, some grid boxes show no data, due in part to the impact of solar contamination in the daytime CALIOP aerosol retrievals. This is exacerbated by the high albedos typically observed in this region compared to other areas in the CONUS (e.g., Houldcroft et al., 2009; Rechid et al., 2009). The lack of data over parts of the western CONUS is also the result of the strict QA protocols, additional screening (cloud-free and dust-free requirements), and data count requirements (> fifty points per grid box) implemented for this study. Note that this data gap

(especially during daytime) over parts of the western CONUS with elevated terrain (e.g., Great Basin and Rockies) is expected and reported in previous studies (e.g., Campbell et al., 2012). This could have resulted from a number of factors, including solar contamination, high surface albedos, QA screening procedures, and surface return contamination/topographic effects. Similar to Fig. 3, and with the same data count requirements discussed previously, $PM_{2.5}$ concentrations derived using nighttime CALIOP aerosol extinction (i.e., the near 0130 UTC equator local-time half-orbital granule) are shown in Fig. 4. Spatial patterns closely resemble those found during daytime, but with no data gaps in the western CONUS (now likely due to the lack of solar influence on the retrievals at night).

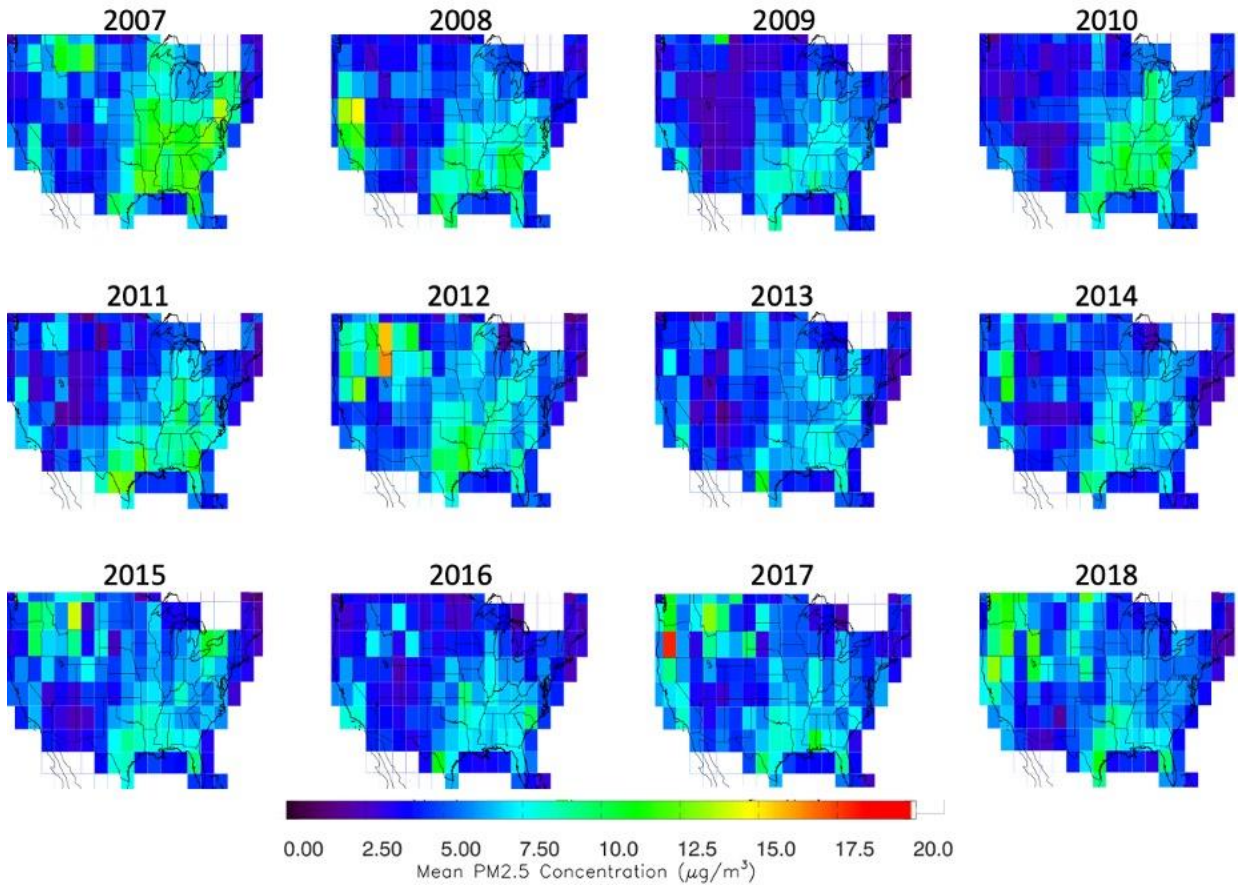

Figure 4. For 2007 to 2018 over the CONUS, 3º x 3º yearly mean $PM_{2.5}$ concentrations derived from nighttime CALIOP near-surface (100-1000 m AGL) aerosol extinction.

Generally, for both daytime and nighttime analyses, a reasonable agreement between the spatial patterns from EPA and those from CALIOP is found (i.e., comparing Fig. 2 with Figs. 3 and 4). Note, however, that the relationship between EPA-based $PM_{2.5}$ and CALIOP-derived $PM_{2.5}$ is explored in a more detailed manner in Sect. 3.2 and 3.3. While some regions and years show better agreement than others, there are instances for which the CALIOP retrieval performs very well. For example, in 2007 over the southeastern CONUS, EPA shows elevated $PM_{2.5}$ concentrations of ~10-15 $\mu g/m^3$, with similar values derived from daytime CALIOP aerosol extinction. For context, the corresponding spatial distributions of 3º x 3º yearly-mean CALIOP-based aerosol extinction from which the $PM_{2.5}$ concentrations were derived are shown in the appendix as Supplemental Figs. 1 (daytime data) and 2 (nighttime data).

Lastly for this section, we evaluate the accuracy of the algorithm for the whole study period by spatially (± 100 km) and temporally (same day) collocating CALIOP-derived $PM_{2.5}$ and $PM_{2.5}$ acquired at EPA stations, following the steps mentioned in Toth et al. (2019). In order to reduce the influence of noise and large extinction uncertainties on the analysis, and to reduce the temporal differences between EPA data (i.e., 24-hour measurements) and CALIOP data (i.e., instantaneous measurements), we compute one-year means of $PM_{2.5}$ concentrations from the EPA and CALIOP. One-year means are also chosen to increase the data counts in our analysis due to the ~16 day repeat cycle of the CALIPSO satellite (i.e., ~22 days of observations per year). Consistent with Toth et al. (2019), only EPA stations with one hundred or more collocated EPA/CALIOP data pairs per year were considered for this analysis. Note that we implement a strict data screening process for which we require all 100 m aerosol extinction bins within the 100-1000 m AGL altitude region to be greater than zero for comparison with EPA $PM_{2.5}$ measurements (again, see Toth et al., 2018 for the impact of zero points on CALIOP-based aerosol averages).

The results of this exercise are shown in Fig. 5, for separate daytime (Fig. 5a) and nighttime (Fig. 5b) analyses and a combined daytime/nighttime analysis (Fig. 5c). Each point in the scatterplots represents a one-year mean $PM_{2.5}$ concentration from the EPA and CALIOP throughout the study period, and a Deming regression was fit to the data (Deming, 1943).

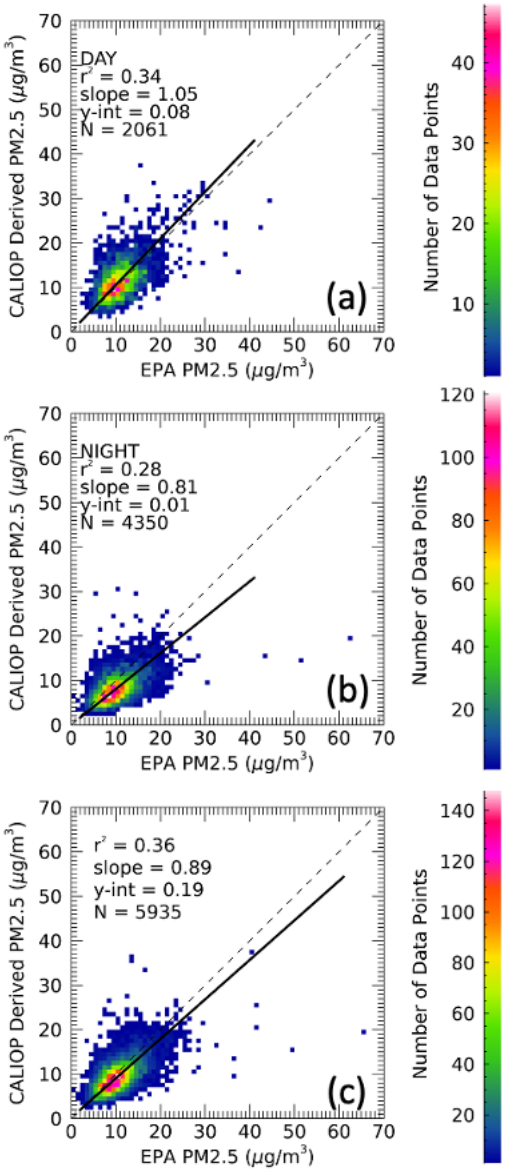

Figure 5. For 2007-2018 over the CONUS, scatterplots of yearly mean $PM_{2.5}$ concentrations from EPA sites and those derived from collocated near-surface CALIOP aerosol extinction, using (a) daytime, (b) nighttime, and (c) combined daytime and nighttime CALIOP data. Points are color-coded by the number of data points per 1 $\mu g/m^3$ bin. The dashed and solid lines show the one-to-one lines and Deming regression fits, respectively.

A slightly better agreement between the two datasets is found for daytime (R^2 = 0.34; Deming slope = 1.05; RMSE = 3.95 μg/m^3; mean bias = 0.62 μg/m^3) compared to nighttime (R^2 = 0.28; Deming slope = 0.81; RMSE = 3.89 μg/m^3; mean bias = -1.99 μg/m^3), with the combined daytime/nighttime analysis yielding the best correlation (R^2 = 0.36; Deming slope = 0.89; RMSE = 3.42 μg/m^3; mean bias = -1.00 μg/m^3).

Considering our temporal (one day) collocation constraint between CALIOP and EPA data points, these R^2 values are higher than the temporal autocorrelation (i.e., R^2 ~0.25 for a 24-hour offset) of aerosols reported in Anderson et al. (2003). For our CALIOP/EPA spatial (100 km) collocation constraint, these R^2 values compare reasonably well with the 100 km spatial autocorrelation of synoptic-scale aerosol plumes (i.e., R^2 of ~0.30) but are smaller than those using all data (i.e., R^2 ~0.64), as presented in Anderson et al. (2003). The larger R^2 value for daytime could be due to the relationship of the CALIOP morning/afternoon retrievals to the ground station observed $PM_{2.5}$ diurnal variability and/or the higher aerosol loadings required for CALIOP aerosol detection during daytime compared to nighttime. It might also be the result of the assumption of the mixed layer height (i.e., 100-100 m AGL) used in this study. These issues are discussed in greater detail in later sections. Figure 5 also shows the data density distributions from 2D histogram computations, as each point is color-coded by the number of points in each 1 μg/m^3 bin. For all three analyses (daytime, nighttime, and combined daytime/nighttime), the peak in data counts occurs at ~ 8-10 μg/m^3.

3.2 Regional analyses

We have further studied regional differences in the mean state and trends of EPA/CALIOP $PM_{2.5}$ concentrations for four arbitrarily partitioned regions as shown in Fig. 1. The yearly mean

341 $PM_{2.5}$ concentrations from EPA (Fig. 2), daytime CALIOP (Fig. 3), and nighttime CALIOP (Fig.
342 4) over the CONUS were used to compute regional means for the following regions: West (≤ -
343 110° longitude), Central (> -110° and ≤ -85° longitude), Northeast (> -85° longitude and ≥ 40°
344 latitude), and Southeast (> -85° longitude and < 40° latitude). We recognize that such large regions
345 will incorporate aerosols from a variety of sources, however a more discrete regional analysis is
346 not the focus of this study.

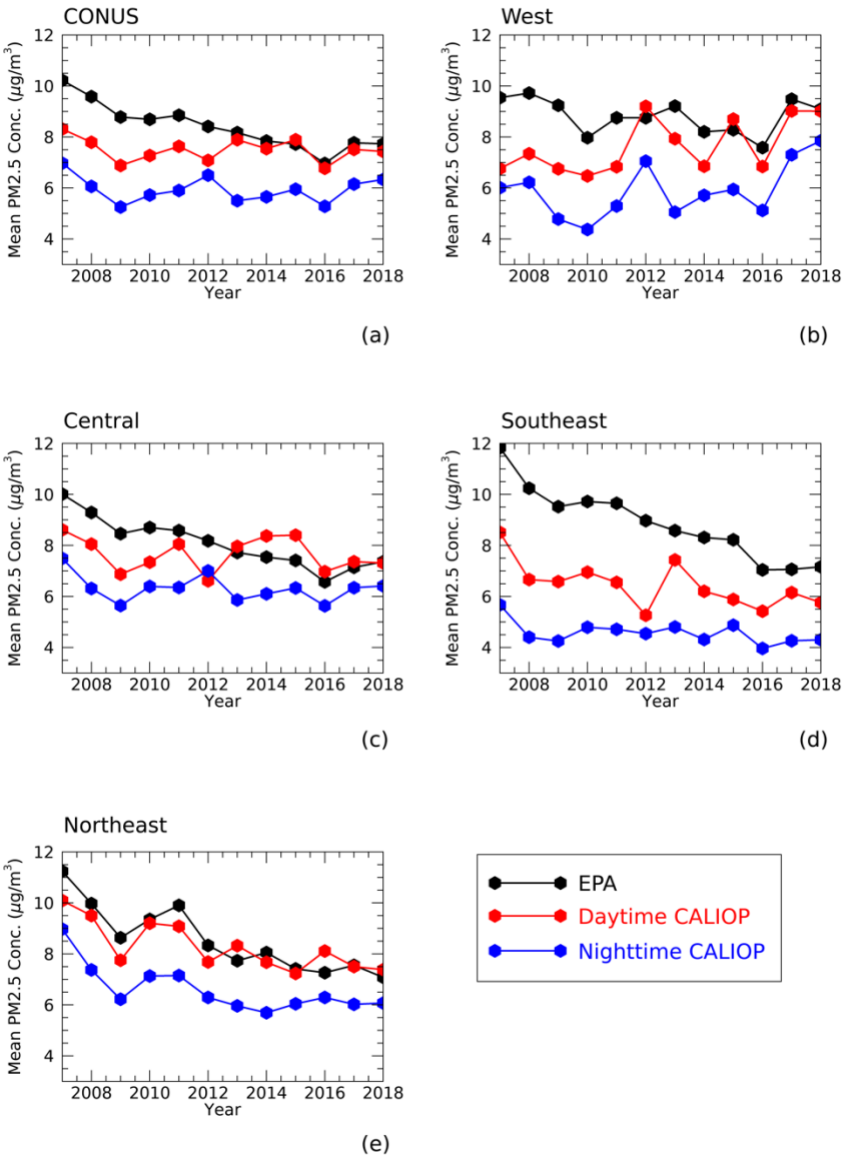

Figure 6. Yearly means of $PM_{2.5}$ concentrations from 2007 to 2018 at EPA stations and derived from daytime and nighttime CALIOP observations for (a) the CONUS and four regions within the CONUS: (b)West, (c) Central, (d) Southeast, and (e) Northeast.

Figure 6 shows the yearly mean regional $PM_{2.5}$ concentrations from EPA (in black), daytime CALIOP (in red), and nighttime CALIOP (in blue) observations for the entire CONUS (Fig. 6a) and four regions: West (Fig. 6b), Central (Fig. 6c), Southeast (Fig. 6d), and Northeast (Fig. 6e). For the CONUS, the yearly mean $PM_{2.5}$ concentrations for EPA more closely match

daytime CALIOP $PM_{2.5}$ than nighttime CALIOP $PM_{2.5}$. Also, nighttime CALIOP $PM_{2.5}$ are consistently smaller than EPA and daytime CALIOP $PM_{2.5}$ for the CONUS throughout the study period, which may plausibly be due to a low bias in near surface CALIOP aerosol extinction at nighttime, or from the diurnal differences in $PM_{2.5}$ concentrations. Both of these patterns for the CONUS are evident for each of the four regions as well.

The region with the largest yearly mean $PM_{2.5}$ differences between the datasets is the Southeast (e.g., 2007, 2008, and 2012). The differences may be attributed to sampling differences between observations from surface stations and CALIOP. It is also possible the differences are caused by retrieval related biases. To further investigate the differences, we compared pair wise the CALIOP-derived yearly mean $PM_{2.5}$ concentrations against those of collocated EPA station data, using methods discussed in Toth et al. (2019) and later in this section, for each of the four regions mentioned above (not shown). CALIOP-EPA $PM_{2.5}$ mean biases on the order of a few $\mu g/m^3$ are found for each region. For example, during daytime, $PM_{2.5}$ mean biases range from ~-0.5 $\mu g/m^3$ (Southeast) to ~2.3 $\mu g/m^3$ (West). During nighttime, mean bias values range from ~-3.5 $\mu g/m^3$ (Southeast) to ~-1.6 $\mu g/m^3$ (Central). These differences are smaller than the differences shown in Fig. 5d, suggesting some of the differences of Fig. 5d are from sampling related biases.

We have also conducted a seasonal analysis of the EPA- and CALIOP- based $PM_{2.5}$ concentrations for the CONUS and the four regions within the CONUS as previously discussed. Monthly mean $PM_{2.5}$ concentrations from each dataset for the 2007-2018 time period are shown in Fig. 7. For the CONUS (Fig. 7a), EPA $PM_{2.5}$ levels are largest in August (~10 $\mu g/m^3$), with elevated levels in December and January and the lowest levels during the spring and fall months. Daytime and nighttime CALIOP-based $PM_{2.5}$ concentrations agree well for May through

September (5-6 μg/m^3). As in the EPA time series, peak daytime $PM_{2.5}$ levels in the CALIOP data are found during wintertime, while the nighttime CALIOP peak occurs in August.

The seasonal patterns observed for the entire CONUS are generally consistent regionally, but $PM_{2.5}$ concentration peaks at higher levels for some regions. For example, in the West (Fig. 7b), the maximum monthly mean $PM_{2.5}$ concentrations is ~12 μg/m^3 in August (e.g., possibly due to the fire season; Mallia et al., 2014) and during December and January. For the Southeast (Fig. 7d), the daytime CALIOP $PM_{2.5}$ peak is ~13 μg/m^3 (occurring in February), and the Northeast region (Fig. 7e) exhibits the most agreement between all three datasets (with $PM_{2.5}$ levels peaking during July).

383

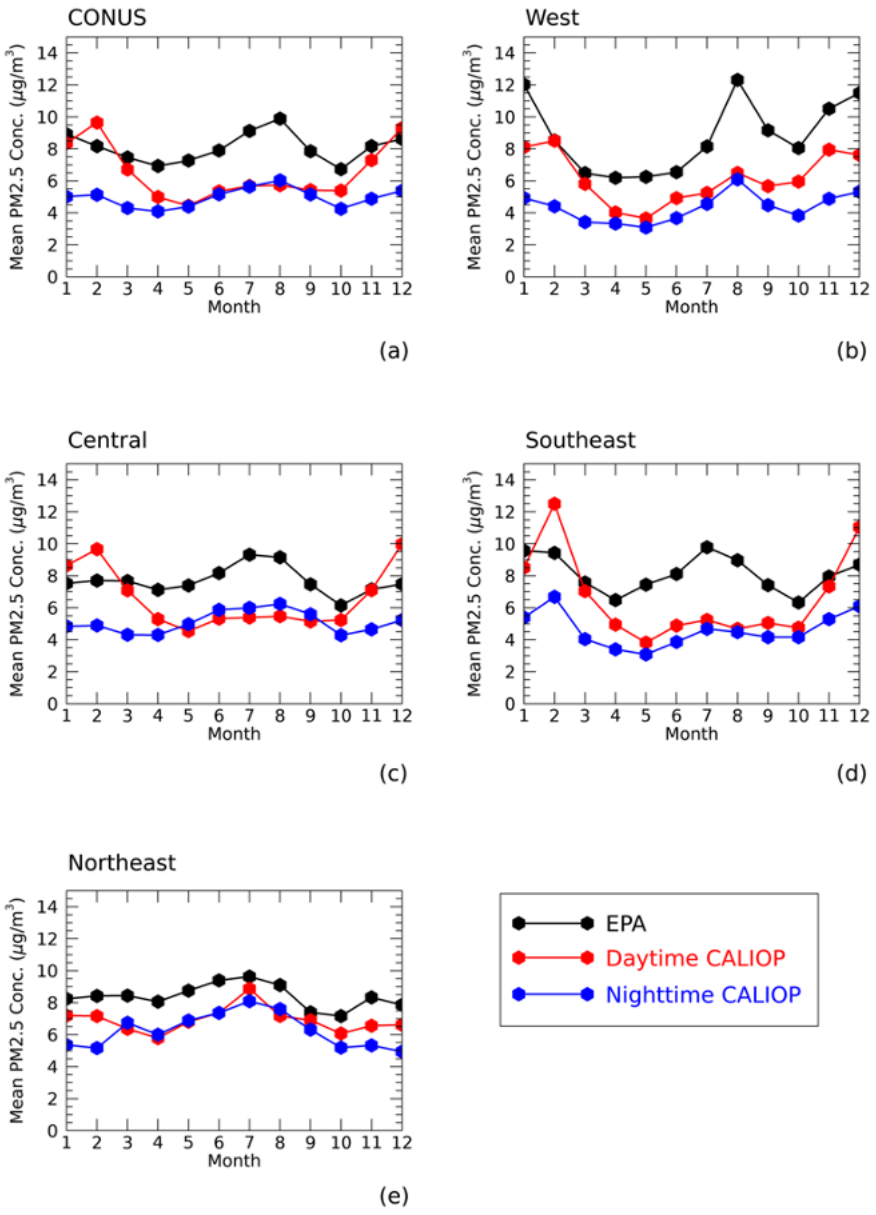

Figure 7. Monthly means of $PM_{2.5}$ concentrations from 2007 to 2018 at EPA stations and derived from daytime and nighttime CALIOP observations for (a) the CONUS and four regions within the CONUS: (b)West, (c) Central, (d) Southeast, and (e) Northeast.

384

385

3.3 Long-term variations of $PM_{2.5}$ from CALIOP and ground-based observations

In this section, the twelve-year mean and trends of EPA and CALIOP-based $PM_{2.5}$ concentrations over the CONUS are explored. Figure 8a shows 3º x 3º mean $PM_{2.5}$ at EPA stations for the twelve-year study period, and the spatial distribution follows the same pattern as discussed earlier in the paper: higher concentrations in the eastern/western CONUS and lower in the central CONUS. The corresponding twelve-year 3º x 3º mean $PM_{2.5}$ concentrations derived from CALIOP are shown in Fig. 8b (daytime CALIOP) and Fig. 8c (nighttime CALIOP).

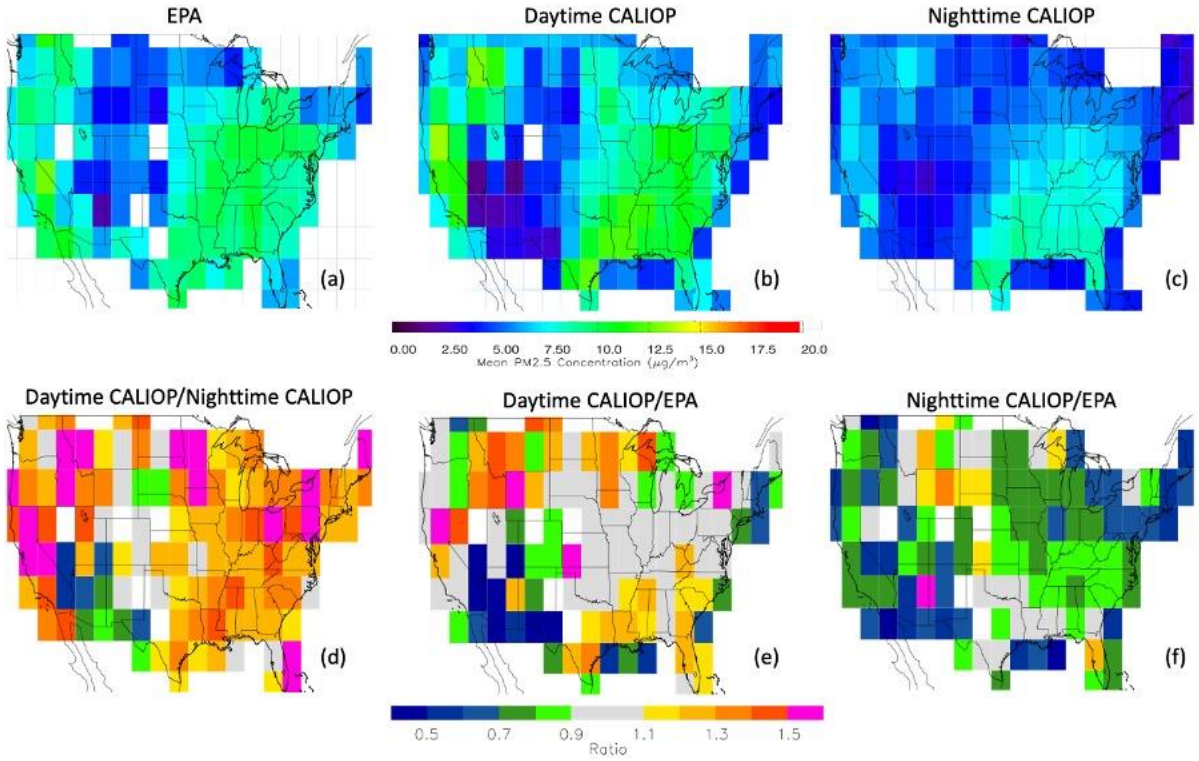

Figure 8. Twelve-year (2007-2018) mean $PM_{2.5}$ concentrations (a) at EPA stations and those derived from (b) daytime, and (c) nighttime, CALIOP near-surface aerosol extinction (gridded at 3º x 3º latitude/longitude resolution). Also shown are the corresponding ratios of (d) daytime to nighttime CALIOP-derived $PM_{2.5}$, (e) daytime CALIOP $PM_{2.5}$ to EPA $PM_{2.5}$, and (f) nighttime CALIOP $PM_{2.5}$ to EPA $PM_{2.5}$, computed for only those grid boxes with available data for each of the analyses in Fig. 8a-c.

Here we require a minimum of 600 points per 3º x 3º grid box (i.e., 50 points per year for 12-year period), and these means include 100-1000 m aerosol extinction equal to zero points. While

daytime CALIOP $PM_{2.5}$ are larger than nighttime CALIOP $PM_{2.5}$, both show similar spatial patterns that match well with that from the EPA. The difference in daytime and nighttime CALIOP-derived $PM_{2.5}$ concentrations is consistent with our past study using two years of CALIOP data (Toth et al., 2019), and is a result of the larger mean near-surface aerosol extinction found over the CONUS during daytime compared to nighttime. While these larger aerosol extinction coefficients may be due to increased aerosol amount near the surface (e.g., from elevated anthropogenic emissions during daytime), solar contamination of the daytime CALIOP aerosol extinction retrieval may also be a factor.

We also computed the corresponding ratios of daytime CALOP-derived $PM_{2.5}$ to nighttime CALIOP-derived $PM_{2.5}$ (Fig. 8d), daytime CALIOP-derived $PM_{2.5}$ to EPA-based $PM_{2.5}$ (Fig. 8e), and nighttime CALIOP-derived $PM_{2.5}$ to EPA-based $PM_{2.5}$ (Fig. 8f), for those grid boxes with available data for each of the analyses (i.e., Fig. 8a-c). Most areas of the CONUS show daytime CALIOP-derived $PM_{2.5}$ concentration estimates larger than those derived from nighttime CALIOP data, with several grid boxes exhibiting ratios greater than 1.5 (Fig. 8d). The exception is for a few grid boxes over the Great Plains and the southwest CONUS, for which daytime CALIOP-derived $PM_{2.5}$ values are smaller than those of nighttime CALIOP-derived $PM_{2.5}$. In terms of the relationship between daytime CALIOP $PM_{2.5}$ and EPA $PM_{2.5}$, many grid boxes with ratios ~ 1 are found throughout the CONUS (Fig. 8e). Southwest CONUS generally exhibits smaller $PM_{2.5}$ concentrations from daytime CALIOP data than EPA observations (likely due to the omission of dust layers from the analysis), otherwise most areas are fairly scattered (i.e., similar number of grid boxes with ratios less than and greater than 1) with no clear regional patterns. However, this not true for the relationship between nighttime CALIOP $PM_{2.5}$ and EPA $PM_{2.5}$, for which most

418 grid boxes exhibit smaller nighttime CALIOP-derived $PM_{2.5}$ concentrations than those from EPA
419 (Fig. 8f).

420 Note that the diurnal variation of $PM_{2.5}$ pollution is dependent on region and season (due
421 in part to meteorology and boundary layer dynamics, e.g., Sun et al., 2013; Chu et al., 2013) and
422 thus may differ even on a site-by-site basis. Furthermore, the CALIOP datasets provide
423 instantaneous estimates of $PM_{2.5}$ concentrations at one time for each daytime and nighttime
424 overpass for a given location. Thus, it is challenging to characterize the expected daytime-
425 nighttime differences in CALIOP-based $PM_{2.5}$ concentrations broadly over the CONUS. The
426 relationship of the $PM_{2.5}$ concentrations estimated at the daytime and nighttime CALIOP overpass
427 times to the EPA-observed $PM_{2.5}$ diurnal variation will be explored in a future study.

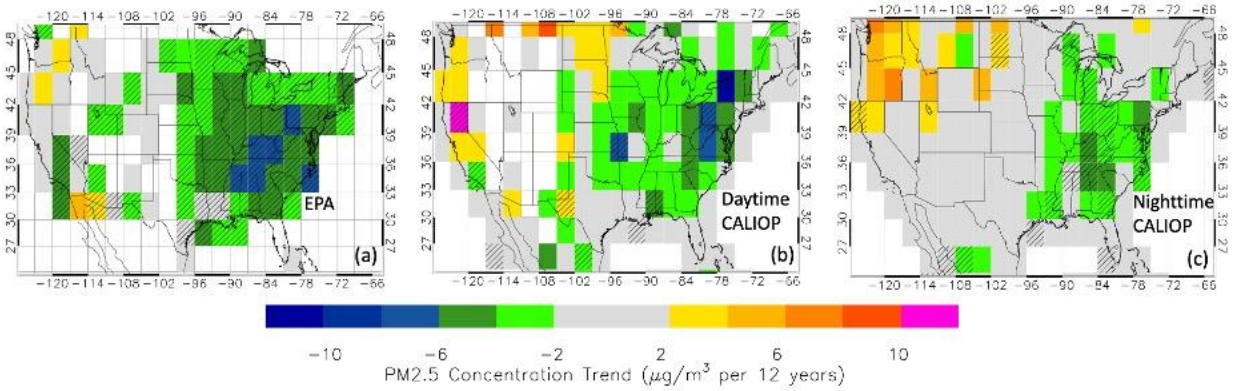

Figure 9. Twelve-year (2007-2018) $PM_{2.5}$ concentration trends (a) at EPA stations and those computed from CALIOP measurements for (b) daytime, and (c) nighttime, conditions (gridded at 3º x 3º latitude/longitude resolution). Hatched grid boxes indicate trends that are significant at the 95% confidence interval, calculated using the Mann-Kendall Test.

428 Figure 9 shows the spatial variability of the 3º x 3º twelve-year trends of $PM_{2.5}$ at EPA
429 stations (Fig. 9a). These trends are computed as the slope from simple linear regression, with the
430 requirement that for a particular grid box every year in the twelve-year period must be represented.
431 If this requirement is not met, no trend is reported. Figure 9a reveals that from 2007 to 2018, most

EPA-based $PM_{2.5}$ concentrations in the eastern CONUS are negative (about -4 to -6 $\mu g/m^3$ per 12 years), indicating an improvement in air quality over the study period. Over the central CONUS, most EPA-reported $PM_{2.5}$ concentrations exhibit slightly negative/near-zero $PM_{2.5}$ trends (i.e., little change in air quality with time). This is generally true for the western CONUS as well, with the exception of some grid boxes in the Pacific Northwest and Southwest that show positive $PM_{2.5}$ trends (about 2-4 $\mu g/m^3$ per 12 years), implying a worsening of air quality from 2007 to 2018 (e.g., due to wildfire activity; McClure and Jaffe, 2018).

Trends for CALIOP-derived $PM_{2.5}$ are shown in Fig. 9b (daytime CALIOP) and Fig. 9c (nighttime CALIOP), computed in the same manner as the EPA analysis, and are only reported if each 3º x 3º grid box included each year in the twelve-year period represented. While the daytime analysis reveals negative $PM_{2.5}$ trends for the eastern CONUS, fewer trends are reported over the western CONUS. The reason for this is the strict data availability requirement implemented for the trend computation, which is a difficult criterion to meet, likely because of terrain effects for the western CONUS and the dust-free requirements. For those grid boxes in the western CONUS with daytime CALIOP trends available, most are positive, especially in California, the Pacific Northwest, and Northern Great Plains. For nighttime (Fig. 9c), the western CONUS reports a far greater number of trend estimates compared to the daytime analysis. While most of these are near zero, positive trends in $PM_{2.5}$ are found over the northwestern CONUS and northern Great Plains. Negative $PM_{2.5}$ trends are found for the eastern CONUS, a result that agrees with the trends computed from both daytime CALIOP data and EPA data. It is noteworthy that the trend patterns discussed here for both EPA and CALIOP are consistent with those values computed using the yearly mean/regional $PM_{2.5}$ concentrations of Fig. 6, as reported in Table 1.

	$PM_{2.5}$ Concentration Trend (μg/m^{3}per 12 years)		
Region	**EPA**	**Daytime CALIOP**	**Nighttime CALIOP**
CONUS	-2.71	-0.39	-0.28
West	-0.77	2.12	1.66
Central	-3.01	-0.51	-0.58
Southeast	-4.58	-1.98	-0.79
Northeast	-3.9	-2.46	-2.25

Table 1. Twelve-year (2007-2018) trends in $PM_{2.5}$ concentrations (μg/m^3) at EPA stations and derived from daytime and nighttime CALIOP observations for the CONUS and four regions within the CONUS: West, Central, Southeast, and Northeast. The trends were computed using the yearly mean $PM_{2.5}$ concentrations shown in Fig. 5.

454

455 The grid boxes of Figs. 9a-9c with a hatched pattern show the locations of statistically
456 significant $PM_{2.5}$ trends from EPA, daytime CALIOP, and nighttime CALIOP, data. The Mann-
457 Kendall test was used (Mann, 1945; Kendall, 1975; Yue et al., 2002; Toth et al., 2016), and we
458 report trends that are significant at the 95% confidence interval. This analysis reveals that the
459 portion of $PM_{2.5}$ trends from EPA data that are statistically significant is considerably greater than
460 that from CALIOP data. This is possibly due to the uncertainties in CALIOP aerosol extinction
461 (e.g., Young et al., 2013; 2018) from which the $PM_{2.5}$ concentrations are derived.

462 To further compare the $PM_{2.5}$ trends between EPA and CALIOP, we focus only on those
463 grid boxes that exhibit statistically significant $PM_{2.5}$ trends from either daytime (Fig. 9b) or
464 nighttime (Fig. 9c) CALIOP data. The results of this analysis are shown in Table 2. For the
465 daytime CALIOP analysis, most CALIOP and EPA $PM_{2.5}$ trends compare well with one another,
466 are negative, and also exhibit statistically significant EPA trends. For the daytime CALIOP
467 analysis, most CALIOP $PM_{2.5}$ trends are negative and compare well with those from EPA data.
468 However, there are two grid boxes that show positive $PM_{2.5}$ trends for both CALIOP and EPA, and

one of which (i.e., the -121.5° longitude midpoint, 40.5° latitude midpoint grid box; northern California) shows a particularly large difference in magnitude (i.e., ~10 $\mu g/m^3$ for CALIOP but ~0 $\mu g/m^3$ for EPA). This is likely due to differences in sampling between the CALIOP and EPA datasets, especially in areas with highly variable terrain (e.g., the valleys, mountains, and forests of northern California). For the nighttime CALIOP analysis, there are a greater number of grid boxes with statistically significant trends, most of which are found in the eastern CONUS, are negative, and agree well with EPA $PM_{2.5}$ trends. Also, note that most of the EPA trends associated with both daytime and nighttime statistically significant CALIOP trends reported in Table 1 are also statistically significant at the 95% CI.

DAYTIME CALIOP ANALYSIS				
		Trend (μg/m^3 per 12 years)		
Longitude Midpoint (deg.)	**Latitude Midpoint (deg.)**	**CALIOP**	**EPA**	**Significant (95% CI) EPA Trend?**
-121.5	40.5	10.55	0.03	No
-118.5	34.5	-3.41	-5.28	Yes
-103.5	31.5	3.82	0.79	No
-94.5	37.5	-6.09	-4.18	Yes
-91.5	28.5	-1.14	-2.23	Yes
-88.5	31.5	-4.30	-3.90	Yes
-79.5	40.5	-7.67	-6.16	Yes
NIGHTTIME CALIOP ANALYSIS				
		Trend (μg/m^3 per 12 years)		
Longitude Midpoint (deg.)	**Latitude Midpoint (deg.)**	**CALIOP**	**EPA**	**Significant (95% CI) EPA Trend?**
-124.5	40.5	2.47	0.01	No
-100.5	46.5	3.47	-2.32	Yes
-94.5	28.5	-1.99	-4.83	Yes
-91.5	31.5	-4.00	-1.84	Yes
-88.5	34.5	-1.94	-6.08	Yes
-88.5	46.5	-3.85	-2.81	Yes
-85.5	34.5	-5.28	-6.48	Yes
-85.5	37.5	-4.67	-6.08	Yes
-85.5	40.5	-2.82	-5.96	Yes
-85.5	43.5	-2.18	-3.26	Yes
-82.5	31.5	-3.66	-4.56	Yes
-82.5	37.5	-3.50	-6.59	Yes
-82.5	40.5	-2.10	-5.55	Yes
-76.5	34.5	-3.89	-6.37	Yes
-76.5	37.5	-3.60	-4.67	Yes

Table 2. The $PM_{2.5}$ trends and their locations for those 3º x 3º grid boxes with statistically significant (95% CI) daytime or nighttime CALIOP $PM_{2.5}$ trends, and the corresponding EPA $PM_{2.5}$ trends, as determined from Fig. 6. The corresponding EPA $PM_{2.5}$ trends that are statistically significant (95% CI) are also indicated.

479

480

Region	$PM_{2.5}$ Concentration Trend (ug/m^3 per 12 years)											
	EPA				Daytime CALIOP				Nighttime CALIOP			
	DJF	MAM	JJA	SON	DJF	MAM	JJA	SON	DJF	MAM	JJA	SON
CONUS	-3.25	-2.86	-2.12	-2.54	-0.88	-0.51	-0.52	0.4	-0.1	-0.77	-0.4	-0.13
West	-2.99	-1.71	2.56	-0.9	-2.75	-0.22	2.53	1.54	0.03	-0.27	2.04	1.04
Central	-3.57	-2.99	-2.41	-3.03	-0.7	-0.89	-0.45	0.01	-0.12	-1.06	-0.46	-0.43
Southeast	-3.36	-3.87	-6.67	-3.87	-0.16	1.27	-3.16	0.39	0.06	0.03	-1.26	-0.23
Northeast	-2.36	-3.84	-6.87	-2.59	-0.81	-2.6	-2.5	-0.29	-0.51	-1.75	-4.35	-1.12

Table 3. Twelve-year (2007-2018) trends in $PM_{2.5}$ concentrations ($\mu g/m^3$) at EPA stations and derived from daytime and nighttime CALIOP observations for the CONUS and four regions within the CONUS for each season: December, January, February (DJF), March, April, May (MAM), June, July, August (JJA), and September, October, November (SON). The trends were computed using the seasonal mean $PM_{2.5}$ concentrations shown in Supplemental Figs. 3-6.

The analyses of this dataset have revealed regional differences in $PM_{2.5}$ trends throughout the CONUS (e.g., Fig. 9 and Table 1). To investigate the reason for these differences, we explore the seasonality of the twelve-year (2007-2018) temporal variations of $PM_{2.5}$ observed at EPA sites and derived from daytime and nighttime CALIOP measurements. Trends were computed from simple linear regression using the seasonal/regional mean $PM_{2.5}$ concentrations provided in the appendix as Supplemental Figs. 3-6. The results of this analysis are shown in Table 3, segmented by region and four seasons: December, January, February (DJF), March, April, May (MAM), June, July, August (JJA), and September, October, November (SON). The majority of regions and seasons exhibit negative $PM_{2.5}$ trends on the order of a few $\mu g/m^3$ to as much as ~ -7 $\mu g/m^3$ (JJA

for Southeast and Northeast). The region that stands out is the West, for which several positive $PM_{2.5}$ trends are found. These positive trends mostly occur during the JJA and SON seasons, but negative trends in $PM_{2.5}$ are found in the West for other seasons. This pattern reveals two important points about the seasonality of $PM_{2.5}$ concentrations for the western CONUS compared to the eastern CONUS. For one, during the more active fire seasons in the West (JJA and SON), $PM_{2.5}$ trends are positive, demonstrating the impact of wildfires on $PM_{2.5}$ concentrations. This likely explains the differences in $PM_{2.5}$ trends for the CONUS as a whole and regionally (e.g., Fig. 9 and Table 1). Second, during the other two seasons (DJF and MAM), $PM_{2.5}$ trends in the West are negative, and thus are in better agreement with the trends exhibited over eastern CONUS. This likely indicates that air quality regulations are functioning in a similar manner for both the eastern and western CONUS.

3.4 Mixed layer height sensitivity studies

The sensitivity of the parameters in Eqn. 3 to the CALIOP retrieved $PM_{2.5}$ concentrations has been explored in Toth et al. (2019), and thus we do not repeat most of the exercises implemented in that paper. Still, consistent with Toth et al. (2019), the mixed layer for this paper is assumed to be 100-1000 m AGL, and thus only CALIOP aerosol extinction in this altitude range is used to derive $PM_{2.5}$ concentrations. The lowest 100 m was not considered due to the possibility of surface contamination in the aerosol retrieval (e.g., Kim et al., 2017). Since only two years of data were used in Toth et al. (2019), we have further tested these analyses using twelve years of the CALIOP data record. Also, we have explored this sensitivity by both considering and excluding the layer nearest the surface (i.e., 0-100 m AGL), as well as extending the surface-height analysis up to 2 km AGL. Also, here we require each 100 m aerosol extinction bin to be greater than zero when varying the height of the assumed mixed layer.

The results of the sensitivity study including the 0-100 m AGL layer are shown in Table 4. In general, varying the height of the mixed layer shows no major changes to the EPA/CALIOP $PM_{2.5}$ relationship for the daytime analysis, with R^2 values around 0.2-0.3 for most layers. However, the smallest R^2 value is found for the 0-100 m layer during nighttime (R^2 = 0.05), corresponding to the largest mean bias (CALIOP-EPA) of about 6.7 µg/m^3. This is consistent with Toth et al. (2019), yet the poor performance of the CALIOP $PM_{2.5}$ retrieval, including whether or not surface return contamination is a factor here, requires further investigation. Contrary to the daytime analysis, the nighttime R^2 values monotonically increase as the mixed layer thickness increases.

Analysis (Day/Night)			
Mixed Layer (m)	**R^2**	**Deming Slope**	**Mean Bias (CALIOP - EPA; µg/m^3)**
0-100	0.23/0.05	1.09/0.56	-2.79/-6.72
0-200	0.27/0.19	1.19/0.72	-0.13/-3.99
0-300	0.29/0.23	1.19/0.77	0.41/-3.23
0-400	0.31/0.25	1.15/0.77	0.40/-2.87
0-500	0.31/0.27	1.12/0.76	0.38/-2.66
0-600	0.31/0.29	1.10/0.74	0.29/-2.56
0-700	0.31/0.29	1.08/0.72	0.30/-2.55
0-800	0.28/0.29	1.08/0.71	0.24/-2.50
0-900	0.25/0.31	1.08/0.74	0.17/-2.45
0-1000	0.26/0.32	1.08/0.75	0.16/-2.45
0-1100	0.30/0.32	1.07/0.77	0.15/-2.43
0-1200	0.29/0.34	1.07/0.75	0.11/-2.45
0-1300	0.26/0.35	1.05/0.74	0.16/-2.46
0-1400	0.23/0.36	1.01/0.74	0.20/-2.43
0-1500	0.24/0.37	1.01/0.75	0.17/-2.45
0-1600	0.25/0.39	1.02/0.76	0.19/-2.41
0-1700	0.26/0.40	1.03/0.76	0.16/-2.41
0-1800	0.27/0.41	1.07/0.79	0.18/-2.28
0-1900	0.23/0.43	1.06/0.80	0.02/-2.28
0-2000	0.22/0.45	1.03/0.78	-0.18/-2.31

Table 4. Results of a sensitivity study varying the height of the assumed mixed layer, including R^2, slope computed from Deming regression analysis, and mean bias (CALIOP – EPA; µg/m^3). This analysis includes the layer nearest the surface (0-100 m).

Table 5 shows the results of the sensitivity study excluding the 0-100 m AGL layer. There is little variability in the EPA/CALIOP $PM_{2.5}$ R^2 values when adjusting the assumed height of the mixed layer for both the daytime and nighttime analyses. However, there is a near monotonic decrease in the daytime CALIOP-EPA bias as the thickness of the assumed mixed layer, yet this pattern not evident in the nighttime biases. We note the results shown in Tables 4 and 5 could be less indicative of the actual aerosol vertical distribution near the surface but more due to the fact

530 that we apply one mixed layer height value for the entire CONUS, in addition to the other reasons
531 discussed below.

Analysis (Day/Night)			
Mixed Layer (m)	**R^2**	**Deming Slope**	**Mean Bias (CALIOP - EPA; µg/m^3)**
100-200	0.23/0.22	1.28/0.94	2.37/-2.67
100-300	0.25/0.24	1.25/0.93	2.16/-2.18
100-400	0.27/0.25	1.19/0.91	1.75/-2.08
100-500	0.28/0.26	1.15/0.88	1.53/-2.00
100-600	0.32/0.27	1.10/0.86	1.24/-1.99
100-700	0.37/0.28	1.04/0.84	1.04/-1.96
100-800	0.35/0.28	1.03/0.82	0.92/-1.96
100-900	0.35/0.29	1.04/0.81	0.71/-1.97
100-1000	0.34/0.28	1.05/0.81	0.62/-1.99
100-1100	0.33/0.30	1.04/0.83	0.58/-2.01
100-1200	0.35/0.31	1.06/0.82	0.46/-2.05
100-1300	0.34/0.33	1.05/0.82	0.47/-2.08
100-1400	0.33/0.34	1.04/0.81	0.46/-2.10
100-1500	0.32/0.35	1.05/0.81	0.43/-2.12
100-1600	0.32/0.35	1.04/0.80	0.37/-2.16
100-1700	0.31/0.35	1.03/0.78	0.35/-2.21
100-1800	0.31/0.34	1.07/0.76	0.31/-2.25
100-1900	0.33/0.34	1.04/0.73	0.06/-2.30
100-2000	0.31/0.32	1.03/0.72	0.05/-2.28

Table 5. Results of a sensitivity study varying the height of the assumed mixed layer, including R^2, slope computed from Deming regression analysis, and mean bias (CALIOP – EPA; µg/m^3). This analysis excludes the layer nearest the surface (0-100 m).

532 We recognize that conducting these sensitivity studies of mixed layer height over the
533 CONUS as a whole is a simplification, as the mixed layer/PBL height varies seasonally and
534 regionally and is dependent upon the local meteorology (e.g., Seidel et al., 2012; Zhang et al.,
535 2020). A more in depth seasonal and regional study of this parameter and its impact on our
536 CALIOP-derived $PM_{2.5}$ estimates is needed. However, the findings of our mixed layer height

sensitivity studies could also be due to aerosol spatial autocorrelation lengths and the EPA/CALIOP collocation limits applied in this study.

For example, by using the data curtain provided by lidars to derive $PM_{2.5}$ concentrations, if the surface term (i.e., 0-100 m) alone is utilized unrestrained, the limited spatial correlation lengths at the surface can negatively impact the surface station/lidar $PM_{2.5}$ relationship. This is especially likely over the complex terrain of the western CONUS, for which shorter EPA surface station - observed $PM_{2.5}$ spatial correlation lengths are found compared to the entire CONUS (Toth et al., 2019). Rather, we might be better served to average extinction to higher altitudes (e.g., 1-2 km AGL), whereby spatial correlation lengths are possibly longer at such heights and thus would characterize near-surface aerosol extinction in a more stable manner, rendering a better comparison and $PM_{2.5}$ product overall.

We note that it is also entirely plausible that the 100 m bin closest to the surface alone is fully accurate, and that the collocation and subsequent analysis applied here are unrepresentative of the actual performance of the 0-100 m bin alone (i.e., if these points were directly collocated, it is possible that the relationship is the inverse of what is shown for this analysis). As Omar et al. (2013) report, however, collocation of ground observations with the CALIOP curtain is challenging. The reader is thus encouraged to consider the context outlined above in interpreting the results of our sensitivity studies and in deciding how exactly to apply either methodology.

3.5 Surface-to-column aerosol representativeness analysis

One assumption under the traditional AOT and $PM_{2.5}$ analyses is that column-integrated AOT can be used to represent near-surface aerosol concentration (e.g., Hoff and Christopher, 2009). Toth et al. (2014) investigated surface-to-column aerosol representativeness using 2 years of CALIOP data and reported a large spatial variation in the fraction of 100-1000 m AOT to the

562 total column AOT. Given the long record of CALIPSO data, it is intriguing to study the temporal
563 variation of the surface-to-column aerosol representativeness as measured by CALIOP. While it
564 is ideal to use CALIOP-derived PBL height estimates here rather than the assumed 100-1000 m
565 AGL layer, this task is challenging, and thus we believe such a topic is best suited for its own
566 paper.

567 Using twelve years of CALIOP cloud-free and dust-free aerosol profile data (i.e., no clouds
568 or dust aerosols identified in the entire atmospheric column), we study the mean state of CALIOP-
569 observed surface-to-column aerosol representativeness over the CONUS. Figure 10a shows the
570 3º x 3º mean fraction of daytime CALIOP 100-1000 m AOT to the total column AOT (%) over
571 the CONUS for the study period. The same data count requirements as Figs. 8b and 8c are
572 implemented for Fig. 10, but with the addition of a near-surface aerosol metric (i.e., the presence
573 of aerosol is required for at least one bin in the 100-1000 m altitude region). We note the lack of
574 daytime data over the western CONUS, due to issues with CALIOP data as discussed earlier in
575 the paper. Over most of the CONUS, the daytime contribution of the AOT below 1 km to the total
576 column AOT is in the neighborhood of 50% to 60% (i.e., roughly consistent with Reid et al., 2017),
577 with the largest contributions occurring in the western CONUS (e.g., California, Oregon, and
578 Washington).

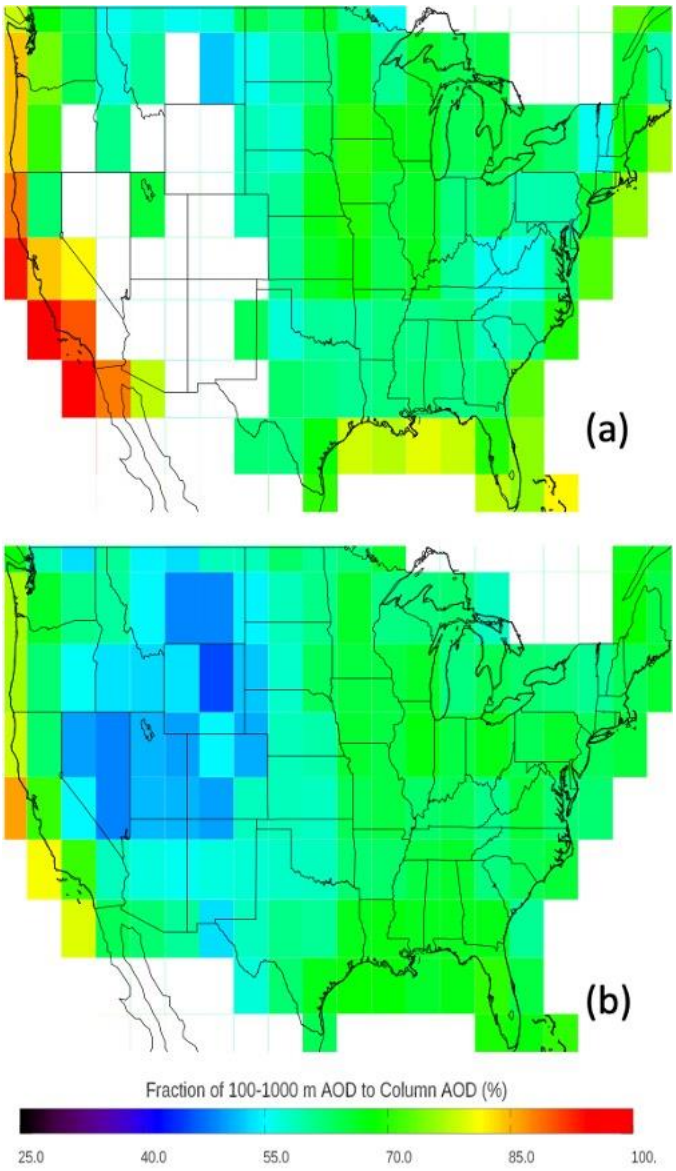

Figure 10. Twelve-year (2007-2018) mean of fraction of 100-1000 m AOD to column AOD (%) on a 3º x 3º grid using (a) daytime and (b) nighttime dust-free CALIOP data.

For the nighttime analysis (Fig. 10b), as during the daytime, percentages around 50-60% are found throughout the CONUS. However, the greater data availability during nighttime over the western CONUS reveals areas with lower percentages (e.g., ~40%-45%). Note that the surface-to-column AOT fractions reported here will be overestimated for those cases for which there is elevated aerosol (e.g., biomass burning smoke) and the CALIOP signal attenuates, due to the near-surface aerosol requirement implemented for this analysis.

Note that we provide yearly mean spatial plots of surface-to-column aerosol representativeness over the CONUS from 2007 to 2018 in Supplemental Fig. 7 (daytime data) and Supplemental Fig. 8 (nighttime data). A more distinct regional spatial pattern is evident in these yearly mean plots, particularly at night, with generally larger percentages in the eastern half of the CONUS compared to the western CONUS. This indicates that aerosol is generally more concentrated near the ground in the eastern CONUS and more vertically diffuse in the western CONUS, a finding consistent with Toth et al. (2014).

The corresponding trends in fraction of 100-1000 m AOT to the total column AOT (% per twelve years) are shown in Supplemental Fig. 9. These were computed with the same procedures and requirements as discussed in Sect. 3.2. As with the previous analyses, the daytime maps show most areas in the western CONUS with no reported trends because of limited data availability in this region (e.g., due to terrain effects and the dust-free requirements), as discussed earlier. While trends of ±10% are found for some grid boxes for both the daytime and nighttime analyses, no clear regional patterns are evident.

4 Conclusions

Using twelve years (2007-2018) of near-surface 532 nm aerosol extinction data from the Cloud-Aerosol Lidar with Orthogonal Polarization (CALIOP) over the contiguous United States (CONUS), particulate matter with aerodynamic diameters smaller than 2.5 μm ($PM_{2.5}$) concentrations were derived from a bulk-mass-modeling-based algorithm that was recently developed from a proof-of-concept study (Toth et al., 2019). The primary goal of this study is to examine the feasibility of applying this newly developed method to nearly the full CALIOP data

607 record and study trends of $PM_{2.5}$ from both CALIOP- and ground station-based $PM_{2.5}$ analyses.
608 We found:

609 1. The spatial distribution of twelve-year mean $PM_{2.5}$ concentrations derived from
610 near-surface CALIOP aerosol data compares well to that of *in situ* $PM_{2.5}$
611 measurements collected at U.S. Environmental Protection Agency (EPA) stations.
612 Using twelve years of combined daytime/nighttime near-surface (100-1000 m)
613 CALIOP data, an encouraging relationship is found between CALIOP-derived
614 $PM_{2.5}$ and EPA-observed $PM_{2.5}$ (Deming slope = 0.89; RMSE = 3.42 $\mu g/m^3$; mean
615 bias = -1.00 $\mu g/m^3$).
616 2. The maps of daytime and nighttime CALIOP-derived $PM_{2.5}$ trends over the
617 CONUS suggest near-zero changes in $PM_{2.5}$ concentrations for many areas, but
618 with a noticeable decreasing pattern in $PM_{2.5}$ over the majority of the eastern
619 CONUS (indicating an improvement in air quality over the 2007-2018 time period),
620 a result consistent with EPA-based $PM_{2.5}$. However, some parts of the western
621 CONUS (e.g., Washington, Oregon, and northern California) show a noticeable
622 increasing pattern in nighttime CALIOP-derived $PM_{2.5}$, but this is not always
623 consistent with daytime CALIOP and EPA-based $PM_{2.5}$, likely due to
624 temporal/spatial sampling differences between the datasets.
625 3. The regionally averaged data over the CONUS (West, Central, Southeast,
626 Northeast) reveals that yearly mean EPA-based $PM_{2.5}$ concentrations more closely
627 match daytime CALIOP-derived $PM_{2.5}$ concentrations than those derived using
628 nighttime CALIOP observations (EPA and daytime $PM_{2.5}$ are larger) for the
629 CONUS and each of the four regions consistently throughout the study period.

Also, agreeable negative trends are found between EPA and CALIOP -based $PM_{2.5}$ concentrations for all regions except the western CONUS, which exhibits positive daytime and nighttime CALIOP $PM_{2.5}$ trends.

4. A seasonal analysis of the EPA and CALIOP $PM_{2.5}$ datasets reveals that over the western CONUS, $PM_{2.5}$ levels trend upward during the more active wildfire season (June through November) but trend downward during other months (December through May). This seasonal pattern demonstrates that the western and eastern CONUS exhibit agreeable negative $PM_{2.5}$ trends over the part of the year for which the western CONUS is not as affected by wildfires, indicative of the air quality regulations implemented in both regions.
5. The assumed mixed layer height in our algorithm is slightly sensitive to the relationship of CALIOP-derived $PM_{2.5}$ to EPA-based $PM_{2.5}$ for the daytime CALIOP analysis but more so for the nighttime CALIOP analysis. Also, the largest daytime and nighttime CALIOP-EPA $PM_{2.5}$ mean biases are found when using only the 0-100 m AGL layer during $PM_{2.5}$ derivation. The poor performance of the algorithm for this layer, and the possible factors impacting it (e.g., surface return contamination), warrant further examination.
6. A noisy spatial distribution of trends in surface-to-column aerosol representativeness, or fraction of 100-1000 m aerosol optical thickness (AOT) to the total column AOT, is exhibited throughout the CONUS.

Accurate monitoring and analysis of surface $PM_{2.5}$ pollution using lidar observations is feasible and has advantages over passive sensor-based methods that use the relationship between AOT and $PM_{2.5}$. While the passive sensor AOT approach is inherently limited by a column-

integrated perspective of aerosol loading, the distribution of aerosols in the atmospheric column can be obtained from lidar measurements (including the near-surface layers that can be used for $PM_{2.5}$ applications). Also, lidar observations provide valuable $PM_{2.5}$ information at nighttime (not achievable using passive sensor data), insight into the vertical distribution of $PM_{2.5}$ pollution, and a source of validation of air quality models. Still, it is challenging to characterize $PM_{2.5}$ concentrations from space-based lidars due to their lack of swath.

Major efforts that remain in developing more robust lidar-based $PM_{2.5}$ estimates include investigating spatial and temporal representativeness issues, analyzing the impact of varying aerosol types and corresponding mass extinction efficiencies (as well as related assumptions such as the removal of dust), and incorporating the mixed layer/planetary boundary layer height as derived from lidar data or provided by models. This study provides compelling motivation to address these challenges and further examine and improve aerosol extinction-based $PM_{2.5}$ concentration retrievals using current and future space-based lidar observations, including the ATLID instrument (do Carmo et al., 2021) on the Earth Clouds, Aerosol, and Radiation Explorer (EarthCARE; Illingworth et al., 2015) satellite, and the lidar instruments associated with the NASA Atmosphere Observing System (AOS), the satellite mission born out of the Aerosols and Clouds, Convection, and Precipitation (ACCP) pre-formulation study (Stephens et al., 2021).

Declaration of competing interest

The authors declare that they have no known competing financial interests or personal relationships that could have appeared to influence the work reported in this paper.

CRediT authorship contribution statement

T.D. Toth: Conceptualization, Methodology, Software, Formal analysis, Investigation, Writing - Original Draft, Writing - Review & Edit, Visualization. **J. Zhang:** Conceptualization, Methodology, Writing - Original Draft, Writing - Review & Edit. **M.A. Vaughan:** Methodology, Writing - Original Draft, Writing - Review & Edit. **J.S. Reid:** Methodology, Writing - Original Draft, Writing - Review & Edit. **J.R. Campbell:** Methodology, Writing - Original Draft, Writing - Review & Edit.

Acknowledgements

This research was funded with the support of the CALIPSO satellite mission. Author JZ acknowledges the support from NASA grants 80NSSC20K1260 and 80NSSC20K1748. Author JSR was supported by the Office of Naval Research Code 322 N0001420WX00481. The Version 4.1 CALIPSO Level 2 5 km aerosol profile (https://doi.org/10.5067/CALIOP/CALIPSO/LID_L2_05KMAPRO-STANDARD-V4-10; last access: 04 October 2021) and aerosol layer (https://doi.org/10.5067/CALIOP/CALIPSO/LID_L2_05KMALAY-STANDARD-V4-10; last access: 04 October 2021) products were obtained from the NASA Langley Research Center Atmospheric Science Data Center. The $PM_{2.5}$ data were obtained from the EPA AQS site

(https://aqs.epa.gov/aqsweb/airdata/download_files.html). The authors also thank Nick Mangus (National Air Data Group, U.S. EPA) for his help with the $PM_{2.5}$ datasets.

References

Anderson, T. L., Charlson, R. J., Winker, D. M., Ogren, J. A., & Holmén, K. (2003). Mesoscale variations of tropospheric aerosols. *Journal of the Atmospheric Sciences*, *60*(1), 119-136, https://doi.org/10.1175/1520-0469(2003)060%3C0119:MVOTA%3E2.0.CO;2.

Bin, C., Song, Z., Pan, F., & Huang, Y. (2021). Obtaining vertical distribution of PM2.5 from CALIOP data and machine learning algorithms. *Science of The Total Environment*, 150338, https://doi.org/10.1016/j.scitotenv.2021.150338.

Campbell, J. R., Tackett, J. L., Reid, J. S., Zhang, J., Curtis, C. A., Hyer, E. J., Sessions, W. R., Westphal, D. L., Prospero, J. M., Welton, E. J., Omar, A. H., Vaughan, M. A., and Winker, D. M. (2012). Evaluating nighttime CALIOP 0.532 μm aerosol optical depth and extinction coefficient retrievals, Atmos. Meas. Tech., 5, 2143–2160, https://doi.org/10.5194/amt-5-2143-2012.

Chen, S. P., Lu, C. H., McQueen, J., & Lee, P. (2018). Application of satellite observations in conjunction with aerosol reanalysis to characterize long-range transport of African and Asian dust on air quality in the contiguous US. *Atmospheric Environment*, *187*, 174-195, https://doi.org/10.1016/j.atmosenv.2018.05.038.

Chow, J. C., Watson, J. G., Park, K., Robinson, N. F., Lowenthal, D. H., Park, K., & Magliano, K. A. (2006). Comparison of particle light scattering and fine particulate matter mass in central California. *Journal of the Air & Waste Management Association*, *56*(4), 398-410, https://doi.org/10.1080/10473289.2006.10464515.

Chu, D. A., Kaufman, Y. J., Zibordi, G., Chern, J. D., Mao, J., Li, C., & Holben, B. N. (2003).

Global monitoring of air pollution over land from the Earth Observing System-Terra Moderate Resolution Imaging Spectroradiometer (MODIS). *Journal of Geophysical Research: Atmospheres*, *108*(D21), https://doi.org/10.1029/2002JD003179.

Chu, D. A., Tsai, T. C., Chen, J. P., Chang, S. C., Jeng, Y. J., Chiang, W. L., & Lin, N. H. (2013). Interpreting aerosol lidar profiles to better estimate surface PM2.5 for columnar AOD measurements. *Atmospheric environment*, *79*, 172-187, https://doi.org/10.1016/j.atmosenv.2013.06.031.

Chung, A., Chang, D. P., Kleeman, M. J., Perry, K. D., Cahill, T. A., Dutcher, D., ... & Stroud, K. (2001). Comparison of real-time instruments used to monitor airborne particulate matter. *Journal of the Air & Waste Management Association*, *51*(1), 109-120, https://doi.org/10.1080/10473289.2001.10464254.

Deming, W. E. (1943). Statistical adjustment of data, Wiley, New York, https://doi.org/10.2307/2086146.

do Carmo, J. P., de Villele, G., Wallace, K., Lefebvre, A., Ghose, K., Kanitz, T., ... & Bravetti, P. (2021). ATmospheric LIDar (ATLID): Pre-Launch Testing and Calibration of the European Space Agency Instrument That Will Measure Aerosols and Thin Clouds in the Atmosphere. *Atmosphere*, *12*(1), 76, https://doi.org/10.3390/atmos12010076.

Eatough, D. J., Long, R. W., Modey, W. K., & Eatough, N. L. (2003). Semi-volatile secondary organic aerosol in urban atmospheres: meeting a measurement challenge. *Atmospheric Environment*, *37*(9-10), 1277-1292, https://doi.org/10.1016/S1352-2310(02)01020-8.

Fang, Z., Yang, H., Zhao, M., Cao, Y., Li, C., Xing, K., ... & Liu, D. (2021). Assessing PM2.5,

766 Aerosol, and Aerosol Optical Depth Concentrations in Hefei Using Modis, Calipso, and
767 Ground-Based Lidar. *Journal of Applied Spectroscopy*, 1-8,
768 https://doi.org/10.1007/s10812-021-01242-z.
769 Ford, B., Val Martin, M., Zelasky, S. E., Fischer, E. V., Anenberg, S. C., Heald, C. L., & Pierce,
770 J. R. (2018). Future fire impacts on smoke concentrations, visibility, and health in the
771 contiguous United States. *GeoHealth*, *2*(8), 229-247,
772 https://doi.org/10.1029/2018GH000144.
773 Gantt, B., McDonald, K., Henderson, B., & Mannshardt, E. (2020). Incorporation of Remote
774 PM2.5 Concentrations into the Downscaler Model for Spatially Fused Air Quality
775 Surfaces. *Atmosphere*, *11*(1), 103, https://doi.org/10.3390/atmos11010103.
776 Greenstone, M. (2002). The impacts of environmental regulations on industrial activity: Evidence
777 from the 1970 and 1977 clean air act amendments and the census of manufactures. *Journal*
778 *of political economy*, *110*(6), 1175-1219, https://doi.org/10.1086/342808.
779 Hand, J. L., & Malm, W. C. (2007). Review of aerosol mass scattering efficiencies from ground-
780 based measurements since 1990. Journal of Geophysical Research, 112, D16203,
781 https://doi.org/10.1029/2007JD008484.
784 Hand, J. L., Prenni, A. J., Copeland, S., Schichtel, B. A., & Malm, W. C. (2020). Thirty years of
785 the Clean Air Act Amendments: Impacts on haze in remote regions of the United States
786 (1990–2018). *Atmospheric Environment*, *243*, 117865,
787 https://doi.org/10.1016/j.atmosenv.2020.117865.
788 Hand, J. L., Schichtel, B. A., Malm, W. C., & Frank, N. H. (2013). Spatial and temporal trends in
789 PM2.5 organic and elemental carbon across the United States. *Advances in*
790 *Meteorology*, *2013*, https://doi.org/10.1155/2013/367674.

Hänel, G. (1976). The properties of atmospheric aerosol particles as functions of the relative humidity at thermodynamic equilibrium with the surrounding moist air. In *Advances in geophysics* (Vol. 19, pp. 73-188). Elsevier, https://doi.org/10.1016/S0065-2687(08)60142-9.

Hess, M., Koepke, P., & Schult, I. (1998). Optical properties of aerosols and clouds: The software package OPAC. *Bulletin of the American meteorological society*, *79*(5), 831-844, https://doi.org/10.1175/1520-0477(1998)079%3C0831:OPOAAC%3E2.0.CO;2.

Hoff, R. M., & Christopher, S. A. (2009). Remote sensing of particulate pollution from space: have we reached the promised land?. *Journal of the Air & Waste Management Association*, *59*(6), 645-675, https://doi.org/10.3155/1047-3289.59.6.645.

Houldcroft, C. J., Grey, W. M., Barnsley, M., Taylor, C. M., Los, S. O., & North, P. R. (2009). New vegetation albedo parameters and global fields of soil background albedo derived from MODIS for use in a climate model. *Journal of Hydrometeorology*, *10*(1), 183-198, https://doi.org/10.1175/2008JHM1021.1.

Illingworth, A. J., Barker, H. W., Beljaars, A., Ceccaldi, M., Chepfer, H., Clerbaux, N., ... & Van Zadelhoff, G. J. (2015). The EarthCARE satellite: The next step forward in global measurements of clouds, aerosols, precipitation, and radiation. *Bulletin of the American Meteorological Society*, *96*(8), 1311-1332, https://doi.org/10.1175/BAMS-D-12-00227.1.

Kaku, K. C., Reid, J. S., Hand, J. L., Edgerton, E. S., Holben, B. N., Zhang, J., & Holz, R. E. (2018). Assessing the challenges of surface-level aerosol mass estimates from remote sensing during the SEAC4RS and SEARCH campaigns: Baseline surface observations and remote sensing in the southeastern United States. *Journal of Geophysical Research: Atmospheres*, *123*(14), 7530-7562, https://doi.org/10.1029/2017JD028074.

Kar, J., Vaughan, M. A., Liu, Z., Omar, A. H., Trepte, C. R., Tackett, J., ... & Kowch, R. (2015). Detection of pollution outflow from Mexico City using CALIPSO lidar measurements. *Remote Sensing of Environment*, *169*, 205-211, https://doi.org/10.1016/j.rse.2015.08.009.

Kendall, M. G. (1975). Rank correlation methods, Griffin, London.

Kim, M. H., Omar, A. H., Vaughan, M. A., Winker, D. M., Trepte, C. R., Hu, Y., ... & Kim, S. W. (2017). Quantifying the low bias of CALIPSO's column aerosol optical depth due to undetected aerosol layers. *Journal of Geophysical Research: Atmospheres*, *122*(2), 1098-1113, https://doi.org/10.1002/2016JD025797.

Kiss, G., Imre, K., Molnár, Á., & Gelencsér, A. (2017). Bias caused by water adsorption in hourly PM measurements. *Atmospheric Measurement Techniques*, *10*, 2477-2484, https://doi.org/10.5194/amt-10-2477-2017.

Kittaka, C., Winker, D. M., Vaughan, M. A., Omar, A., & Remer, L. A. (2011). Intercomparison of column aerosol optical depths from CALIPSO and MODIS-Aqua. *Atmospheric Measurement Techniques*, *4*(2), 131, https://doi.org/10.5194/amt-4-131-2011.

Lee, H. J., Coull, B. A., Bell, M. L., & Koutrakis, P. (2012). Use of satellite-based aerosol optical depth and spatial clustering to predict ambient PM2.5 concentrations. *Environmental research*, *118*, 8-15, https://doi.org/10.1016/j.envres.2012.06.011.

Liou, K. N. (2002). *An introduction to atmospheric radiation*. Elsevier.

Liu, Y., Park, R. J., Jacob, D. J., Li, Q., Kilaru, V., & Sarnat, J. A. (2004). Mapping annual mean ground-level PM2.5 concentrations using Multiangle Imaging Spectroradiometer aerosol optical thickness over the contiguous United States. *Journal of Geophysical Research: Atmospheres*, *109*(D22), https://doi.org/10.1029/2004JD005025.

Lynch, P., Reid, J. S., Westphal, D. L., Zhang, J., Hogan, T. F., Hyer, E. J., ... & Rubin, J. I. (2016). An 11-year global gridded aerosol optical thickness reanalysis (v1. 0) for atmospheric and climate sciences. *Geoscientific Model Development*, *9*(4), https://doi.org/10.5194/gmd-9-1489-2016.

Mallia, D. V., Lin, J. C., Urbanski, S., Ehleringer, J., & Nehrkorn, T. (2015). Impacts of upwind wildfire emissions on CO, CO2, and PM2. 5 concentrations in Salt Lake City, Utah. *Journal of Geophysical Research: Atmospheres*, *120*(1), 147-166, https://doi.org/10.1002/2014JD022472.

Malm, W.C. and Hand, J.L. (2007). An examination of the physical and optical properties of aerosols collected in the IMPROVE program. Atmospheric Environment, 41(16), pp.3407-3427, https://doi.org/10.1016/j.atmosenv.2006.12.012.

Mann, H. B. (1945). Nonparametric tests against trend. *Econometrica: Journal of the econometric society*, 245-259, https://doi.org/10.2307/1907187.

McClure, C. D., & Jaffe, D. A. (2018). US particulate matter air quality improves except in wildfire-prone areas. *Proceedings of the National Academy of Sciences*, *115*(31), 7901-7906, https://doi.org/10.1073/pnas.1804353115.

National Academies of Sciences, Engineering, and Medicine. 2018. Thriving on Our Changing Planet: A Decadal Strategy for Earth Observation from Space. Washington, DC: The National Academies Press. https://doi.org/10.17226/24938.

Noble, C. A., Vanderpool, R. W., Peters, T. M., McElroy, F. F., Gemmill, D. B., & Wiener, R. W. (2001). Federal reference and equivalent methods for measuring fine particulate matter. *Aerosol science & technology*, *34*(5), 457-464, https://doi.org/10.1080/02786820121582.

Omar, A. H., Winker, D. M., Tackett, J. L., Giles, D. M., Kar, J., Liu, Z., ... & Trepte, C. R. (2013). CALIOP and AERONET aerosol optical depth comparisons: One size fits none. *Journal of Geophysical Research: Atmospheres*, *118*(10), 4748-4766, https://doi.org/10.1002/jgrd.50330.

Omar, A. H., Winker, D. M., Vaughan, M. A., Hu, Y., Trepte, C. R., Ferrare, R. A., ... & Liu, Z. (2009). The CALIPSO automated aerosol classification and lidar ratio selection algorithm. *Journal of Atmospheric and Oceanic Technology*, *26*(10), 1994-2014, https://doi.org/10.1175/2009JTECHA1231.1.

Omar, A. H., Won, J. G., Winker, D. M., Yoon, S. C., Dubovik, O., & McCormick, M. P. (2005). Development of global aerosol models using cluster analysis of Aerosol Robotic Network (AERONET) measurements. *Journal of Geophysical Research: Atmospheres*, *110*(D10), https://doi.org/10.1029/2004JD004874.

Padgett, J., & Richmond, H. (1983). The process of establishing and revising national ambient air quality standards. *Journal of the Air Pollution Control Association*, *33*(1), 13-16, https://doi.org/10.1080/00022470.1983.10465541.

Patashnick, H., Rupprecht, G., Ambs, J. L., & Meyer, M. B. (2001). Development of a reference standard for particulate matter mass in ambient air. *Aerosol Science & Technology*, *34*(1), 42-45, https://doi.org/10.1080/02786820117268.

Pope Iii, C. A., Burnett, R. T., Thun, M. J., Calle, E. E., Krewski, D., Ito, K., & Thurston, G. D. (2002). Lung cancer, cardiopulmonary mortality, and long-term exposure to fine particulate air pollution. *Jama*, *287*(9), 1132-1141, https://doi.org/10.1001/jama.287.9.1132.

Rechid, D., Raddatz, T. J., & Jacob, D. (2009). Parameterization of snow-free land surface albedo

as a function of vegetation phenology based on MODIS data and applied in climate modelling. *Theoretical and applied Climatology*, *95*(3), 245-255, https://doi.org/10.1007/s00704-008-0003-y.

Reid, J. S., Kuehn, R. E., Holz, R. E., Eloranta, E. W., Kaku, K. C., Kuang, S., et al. (2017). Ground-based high spectral resolution lidar observation of aerosol vertical distribution in the summertime southeast United States. Journal of Geophysical Research: Atmospheres, 122, 2970–3004, https://doi.org/10.1002/2016JD025798.

Schwartz, J., Dockery, D. W., & Neas, L. M. (1996). Is daily mortality associated specifically with fine particles?. *Journal of the Air & Waste Management Association*, *46*(10), 927-939, https://doi.org/10.1080/10473289.1996.10467528.

Seidel, D. J., Zhang, Y., Beljaars, A., Golaz, J. C., Jacobson, A. R., & Medeiros, B. (2012). Climatology of the planetary boundary layer over the continental United States and Europe. *Journal of Geophysical Research: Atmospheres*, *117*(D17), https://doi.org/10.1029/2012JD018143.

Spagnolo, G. S. (1989). Automatic instrument for aerosol samples using the beta-particle attenuation. *Journal of aerosol science*, *20*(1), 19-27, https://doi.org/10.1016/00218502(87)90151-0.

Stephens, G., Kalashnikova, O., Gristey, J. J., Pilewskie, P., Thompson, D. R., Huang, X., ... & Schmidt, S. (2021). The spectral nature of Earth's reflected radiation: measurement and science applications. *Front. Remote Sens. 2: 664291*, https://doi.org/10.3389/frsen.2021.664291.

Stephens, G., Winker, D., Pelon, J., Trepte, C., Vane, D., Yuhas, C., ... & Lebsock, M. (2018).

905 CloudSat and CALIPSO within the A-Train: Ten years of actively observing the Earth
906 system. *Bulletin of the American Meteorological Society*, *99*(3), 569-581,
907 https://doi.org/10.1175/BAMS-D-16-0324.1.
908 Sun, Y., Song, T., Tang, G., & Wang, Y. (2013). The vertical distribution of PM2.5 and boundary-
909 layer structure during summer haze in Beijing. *Atmospheric Environment*, *74*, 413-421,
910 https://doi.org/10.1016/j.atmosenv.2013.03.011.
911 Tao, M., Chen, L., Su, L., & Tao, J. (2012). Satellite observation of regional haze pollution over
912 the North China Plain. *Journal of Geophysical Research: Atmospheres*, *117*(D12),
913 https://doi.org/10.1029/2012JD017915.
914 Tosca, M. G., Campbell, J., Garay, M., Lolli, S., Seidel, F. C., Marquis, J., & Kalashnikova, O.
915 (2017). Attributing accelerated summertime warming in the southeast united states to
916 recent reductions in aerosol burden: Indications from vertically-resolved
917 observations. *Remote Sensing*, *9*(7), 674, https://doi.org/10.3390/rs9070674.
918 Toth, T. D., Campbell, J. R., Reid, J. S., Tackett, J. L., Vaughan, M. A., Zhang, J., & Marquis, J.
919 W. (2018). Minimum aerosol layer detection sensitivities and their subsequent impacts on
920 aerosol optical thickness retrievals in CALIPSO level 2 data products. *Atmospheric*
921 *measurement techniques*, *11*(1), 499-514, https://doi.org/10.5194/amt-11-499-2018.
922 Toth, T. D., Zhang, J., Campbell, J. R., Hyer, E. J., Reid, J. S., Shi, Y., & Westphal, D. L. (2014).
923 Impact of data quality and surface-to-column representativeness on the PM2.5/satellite
924 AOD relationship for the contiguous United States. *Atmospheric Chemistry &*
925 *Physics*, *14*(12), https://doi.org/10.5194/acp-14-6049-2014.
926 Toth, T. D., Zhang, J., Campbell, J. R., Reid, J. S., & Vaughan, M. A. (2016). Temporal variability

927 of aerosol optical thickness vertical distribution observed from CALIOP. *Journal of*
928 *Geophysical Research: Atmospheres*, *121*(15), 9117-9139,
929 https://doi.org/10.1002/2015JD024668.
930 Toth, T. D., Zhang, J., Reid, J. S., and Vaughan, M. A. (2019). A bulk-mass-modeling-based
931 method for retrieving particulate matter pollution using CALIOP observations, Atmos.
932 Meas. Tech., 12, 1739–1754, https://doi.org/10.5194/amt-12-1739-2019.
933 US Environmental Protection Agency. (1997). National ambient air quality standards for
934 particulate matter: Final rule. *Fed. Regist.*, *62*(138), 38-651.
935 U.S. Environmental Protection Agency, 2020, Reviewing National Ambient Air Quality Standards
936 (NAAQS): Scientific and Technical Information, Retrieved on February 27, 2020 from
937 https://www.epa.gov/naaqs/.
938 Van Donkelaar, A., Martin, R. V., Brauer, M., Hsu, N. C., Kahn, R. A., Levy, R. C., ... & Winker,
939 D. M. (2016). Global estimates of fine particulate matter using a combined geophysical-
940 statistical method with information from satellites, models, and monitors. *Environmental*
941 *science & technology*, *50*(7), 3762-3772, https://doi.org/10.1021/acs.est.5b05833.
942 Van Donkelaar, A., Martin, R. V., & Park, R. J. (2006). Estimating ground-level PM2.5 using
943 aerosol optical depth determined from satellite remote sensing. *Journal of Geophysical*
944 *Research: Atmospheres*, *111*(D21), https://doi.org/10.1029/2005JD006996.
945 Wang, J., & Christopher, S. A. (2003). Intercomparison between satellite-derived aerosol optical
946 thickness and PM2.5 mass: Implications for air quality studies. *Geophysical research*
947 *letters*, *30*(21), https://doi.org/10.1029/2003GL018174.
948 Winker, D. M., Pelon, J., Coakley Jr, J. A., Ackerman, S. A., Charlson, R. J., Colarco, P. R., ... &

Kubar, T. L. (2010). The CALIPSO mission: A global 3D view of aerosols and clouds. *Bulletin of the American Meteorological Society*, *91*(9), 1211-1230, https://doi.org/10.1175/2010BAMS3009.1.

Winker, D. M., Tackett, J. L., Getzewich, B. J., Liu, Z., Vaughan, M. A., & Rogers, R. R. (2013). The global 3-D distribution of tropospheric aerosols as characterized by CALIOP. *Atmospheric Chemistry & Physics*, *13*(6), https://doi.org/10.5194/acp-13-3345-2013.

Xie, Y., Wang, Y., Zhang, K., Dong, W., Lv, B., & Bai, Y. (2015). Daily estimation of ground-level PM2.5 concentrations over Beijing using 3 km resolution MODIS AOD. *Environmental science & technology*, *49*(20), 12280-12288, https://doi.org/10.1021/acs.est.5b01413.

Xing, Y. F., Xu, Y. H., Shi, M. H., & Lian, Y. X. (2016). The impact of PM2.5 on the human respiratory system. *Journal of thoracic disease*, *8*(1), E69, https://dx.doi.org/10.3978%2Fj.issn.2072-1439.2016.01.19.

Yeom, J. M., Roujean, J. L., Han, K. S., Lee, K. S., & Kim, H. W. (2020). Thin cloud detection over land using background surface reflectance based on the BRDF model applied to Geostationary Ocean Color Imager (GOCI) satellite data sets. *Remote Sensing of Environment*, *239*, 111610, https://doi.org/10.1016/j.rse.2019.111610.

Yin, X., Kang, S., Rupakheti, M., de Foy, B., Li, P., Yang, J., ... & Rupakheti, D. (2021). Influence of transboundary air pollution on air quality in southwestern China. *Geoscience Frontiers*, *12*(6), 101239, https://doi.org/10.1016/j.gsf.2021.101239.

Young, S. A., Vaughan, M. A., Garnier, A., Tackett, J. L., Lambeth, J. D., & Powell, K. A. (2018).

Extinction and optical depth retrievals for CALIPSO's Version 4 data release. Atmospheric Measurement Techniques, 11(10), 5701-5727, https://doi.org/10.5194/amt-11-5701-2018.

Young, S. A., Vaughan, M. A., Kuehn, R. E., & Winker, D. M. (2013). The retrieval of profiles of particulate extinction from Cloud–Aerosol Lidar and Infrared Pathfinder Satellite Observations (CALIPSO) data: Uncertainty and error sensitivity analyses. Journal of Atmospheric and Oceanic Technology, 30(3), 395-428, https://doi.org/10.1175/JTECH-D-12-00046.1.

Yue, S., Pilon, P., Phinney, B., & Cavadias, G. (2002). The influence of autocorrelation on the ability to detect trend in hydrological series. *Hydrological processes*, *16*(9), 1807-1829, https://doi.org/10.1002/hyp.1095.

Zhang, Y., Sun, K., Gao, Z., Pan, Z., Shook, M. A., & Li, D. (2020). Diurnal climatology of planetary boundary layer height over the contiguous United States derived from AMDAR and reanalysis data. *Journal of Geophysical Research: Atmospheres*, *125*(20), https://doi.org/10.1029/2020JD032803.

Figure and Table Captions

Figure 1. Map of the CONUS showing the locations of U.S. EPA stations that report daily $PM_{2.5}$ concentration observations (Parameter Code: 88101) during the study time period (2007-2018). The red lines delineate the boundaries of four regions: West (≤ -110° longitude), Central (> -110° and ≤ -85° longitude), Northeast (> -85° longitude and ≥ 40° latitude), and Southeast (> -85° longitude and < 40° latitude).

Figure 2. For 2007 to 2018, yearly mean $PM_{2.5}$ concentrations, computed from daily measurements and gridded at 3º x 3º latitude/longitude resolution, from EPA sites across the CONUS.

Figure 3. For 2007 to 2018 over the CONUS, 3º x 3º yearly mean $PM_{2.5}$ concentrations derived from daytime CALIOP near-surface (100-1000 m AGL) aerosol extinction.

Figure 4. For 2007 to 2018 over the CONUS, 3º x 3º yearly mean $PM_{2.5}$ concentrations derived from nighttime CALIOP near-surface (100-1000 m AGL) aerosol extinction.

Figure 5. For 2007-2018 over the CONUS, scatterplots of yearly mean $PM_{2.5}$ concentrations from EPA sites and those derived from collocated near-surface CALIOP aerosol extinction, using (a) daytime, (b) nighttime, and (c) combined daytime and nighttime CALIOP data. Points are color-coded by the number of data points per 1 $\mu g/m^3$ bin. The dashed and solid lines show the one-to-one lines and Deming regression fits, respectively.

1027 Figure 6. Yearly means of $PM_{2.5}$ concentrations from 2007 to 2018 at EPA stations and derived
1028 from daytime and nighttime CALIOP observations for (a) the CONUS and four regions within the
1029 CONUS: (b)West, (c) Central, (d) Southeast, and (e) Northeast.
1030
1031 Figure 7. Monthly means of $PM_{2.5}$ concentrations from 2007 to 2018 at EPA stations and derived
1032 from daytime and nighttime CALIOP observations for (a) the CONUS and four regions within the
1033 CONUS: (b)West, (c) Central, (d) Southeast, and (e) Northeast.
1034
1035 Figure 8. Twelve-year (2007-2018) mean $PM_{2.5}$ concentrations (a) at EPA stations and those
1036 derived from (b) daytime, and (c) nighttime, CALIOP near-surface aerosol extinction (gridded at
1037 3º x 3º latitude/longitude resolution). Also shown are the corresponding ratios of (d) daytime to
1038 nighttime CALIOP-derived $PM_{2.5}$, (e) daytime CALIOP $PM_{2.5}$ to EPA $PM_{2.5}$, and (f) nighttime
1039 CALIOP $PM_{2.5}$ to EPA $PM_{2.5}$, computed for only those grid boxes with available data for each of
1040 the analyses in Fig. 8a-c.
1041
1042 Figure 9. Twelve-year (2007-2018) $PM_{2.5}$ concentration trends (a) at EPA stations and those
1043 computed from CALIOP measurements for (b) daytime, and (c) nighttime, conditions (gridded at
1044 3º x 3º latitude/longitude resolution). Hatched grid boxes indicate trends that are significant at the
1045 95% confidence interval, calculated using the Mann-Kendall Test.
1046
1047 Figure 10. Twelve-year (2007-2018) mean of fraction of 100-1000 m AOD to column AOD (%)
1048 on a 3º x 3º grid using (a) daytime and (b) nighttime dust-free CALIOP data.
1049

Table 1. Twelve-year (2007-2018) trends in $PM_{2.5}$ concentrations ($\mu g/m^3$) at EPA stations and derived from daytime and nighttime CALIOP observations for the CONUS and four regions within the CONUS: West, Central, Southeast, and Northeast. The trends were computed using the yearly mean $PM_{2.5}$ concentrations shown in Fig. 5.

Table 2. The $PM_{2.5}$ trends and their locations for those 3º x 3º grid boxes with statistically significant (95% CI) daytime or nighttime CALIOP $PM_{2.5}$ trends, and the corresponding EPA $PM_{2.5}$ trends, as determined from Fig. 6. The corresponding EPA $PM_{2.5}$ trends that are statistically significant (95% CI) are also indicated.

Table 3. Twelve-year (2007-2018) trends in $PM_{2.5}$ concentrations ($\mu g/m^3$) at EPA stations and derived from daytime and nighttime CALIOP observations for the CONUS and four regions within the CONUS for each season: December, January, February (DJF), March, April, May (MAM), June, July, August (JJA), and September, October, November (SON). The trends were computed using the seasonal mean $PM_{2.5}$ concentrations shown in Supplemental Figs. 3-6.

Table 4. Results of a sensitivity study varying the height of the assumed mixed layer, including R^2, slope computed from Deming regression analysis, and mean bias (CALIOP – EPA; $\mu g/m^3$). This analysis includes the layer nearest the surface (0-100 m).

Table 5. Results of a sensitivity study varying the height of the assumed mixed layer, including R^2, slope computed from Deming regression analysis, and mean bias (CALIOP – EPA; $\mu g/m^3$). This analysis excludes the layer nearest the surface (0-100 m).

Supplemental Figure 1. For 2007 to 2018 over the CONUS, 3º x 3º yearly mean aerosol extinction (100-1000 m layer AGL) derived from daytime CALIOP measurements.

Supplemental Figure 2. For 2007 to 2018 over the CONUS, 3º x 3º yearly mean aerosol extinction (100-1000 m layer AGL) derived from nighttime CALIOP measurements.

Supplemental Figure 3. Seasonal means (December through February) of $PM_{2.5}$ concentrations for each year from 2007 to 2018 at EPA stations and derived from daytime and nighttime CALIOP observations for (a) the CONUS and four regions within the CONUS: (b)West, (c) Central, (d) Southeast, and € Northeast.

Supplemental Figure 4. Seasonal means (March through May) of $PM_{2.5}$ concentrations for each year from 2007 to 2018 at EPA stations and derived from daytime and nighttime CALIOP observations for (a) the CONUS and four regions within the CONUS: (b)West, (c) Central, (d) Southeast, and (e) Northeast.

Supplemental Figure 5. Seasonal means (July through August) of $PM_{2.5}$ concentrations for each year from 2007 to 2018 at EPA stations and derived from daytime and nighttime CALIOP observations for (a) the CONUS and four regions within the CONUS: (b)West, (c) Central, (d) Southeast, and € Northeast.

Supplemental Figure 6. Seasonal means (September through November) of $PM_{2.5}$ concentrations for each year from 2007 to 2018 at EPA stations and derived from daytime and nighttime CALIOP observations for (a) the CONUS and four regions within the CONUS: (b)West, (c) Central, (d) Southeast, and (e) Northeast.

Supplemental Figure 7. For 2007 to 2018 over the CONUS, 3º x 3º yearly mean fraction of 100-1000 m AOD to column AOD (%) as observed by CALIOP during dust-free daytime conditions.

Supplemental Figure 8. For 2007 to 2018 over the CONUS, 3º x 3º yearly mean fraction of 100-1000 m AOD to column AOD (%) as observed by CALIOP during dust-free nighttime conditions.

Supplemental Figure 9. Twelve-year (2007-2018) trends of fraction of 100-1000 m AOD to column AOD (% per twelve years) on a 3º x 3º grid using (a) daytime and (b) nighttime dust-free CALIOP data.

Appendices

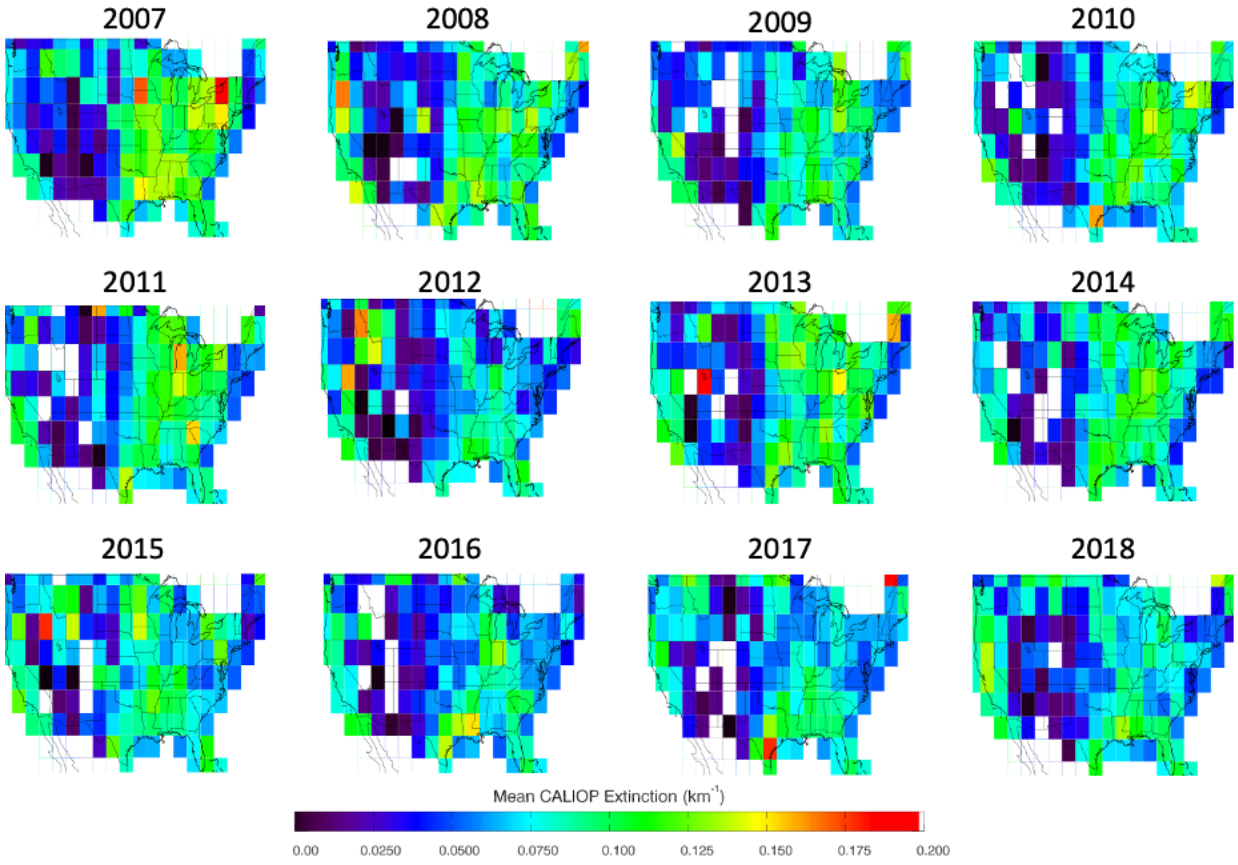

Supplemental Figure 1. For 2007 to 2018 over the CONUS, 3º x 3º yearly mean aerosol extinction (100-1000 m layer AGL) derived from daytime CALIOP measurements.

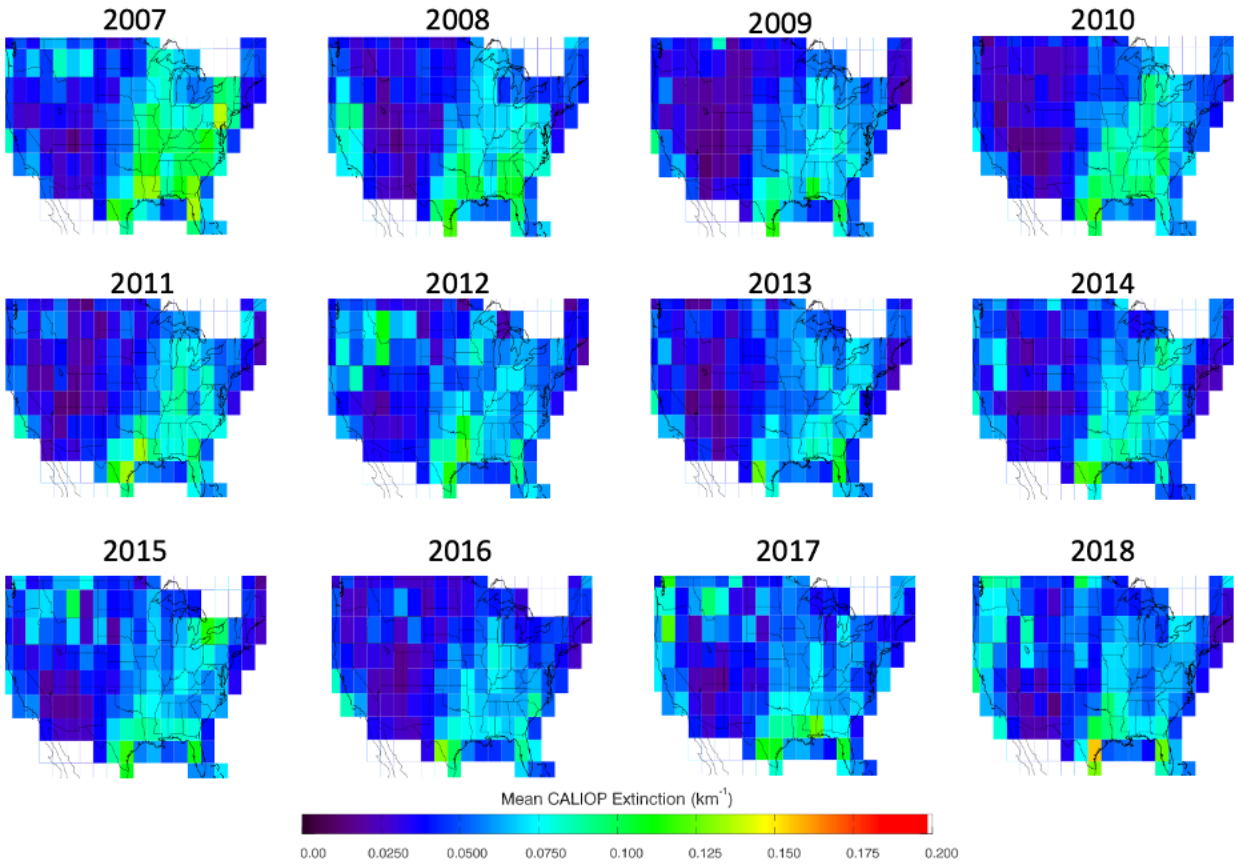

Supplemental Figure 2. For 2007 to 2018 over the CONUS, 3º x 3º yearly mean aerosol extinction (100-1000 m layer AGL) derived from nighttime CALIOP measurements.

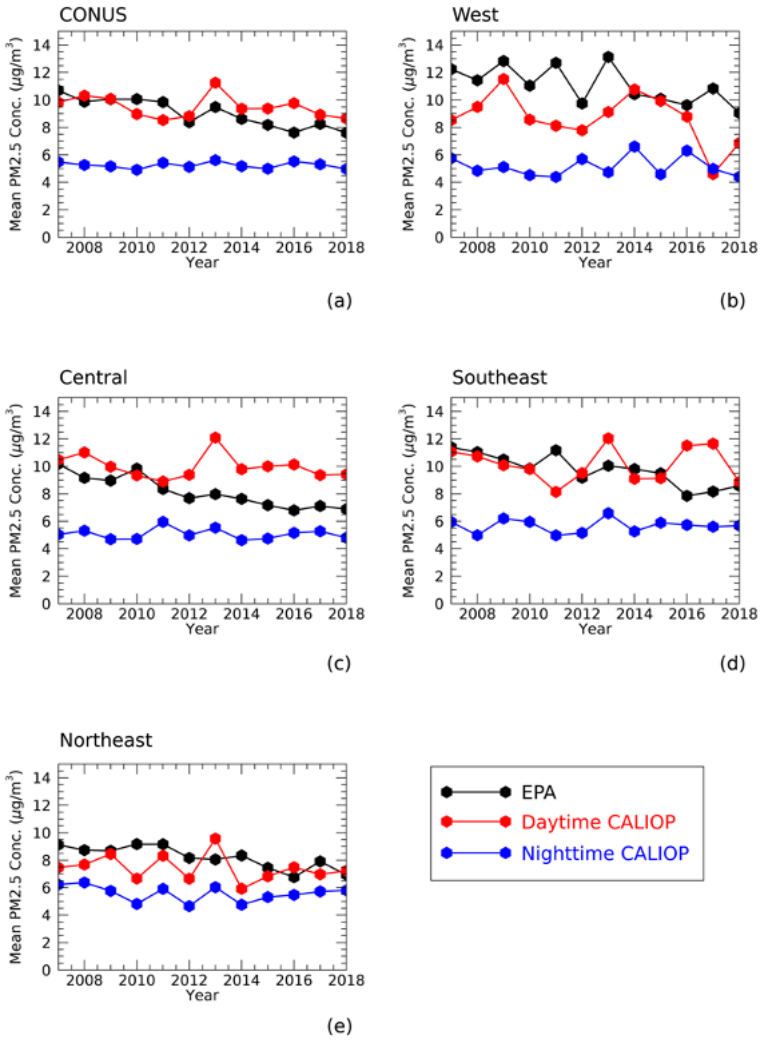

Supplemental Figure 3. Seasonal means (December through February) of $PM_{2.5}$ concentrations for each year from 2007 to 2018 at EPA stations and derived from daytime and nighttime CALIOP observations for (a) the CONUS and four regions within the CONUS: (b)West, (c) Central, (d) Southeast, and (e) Northeast.

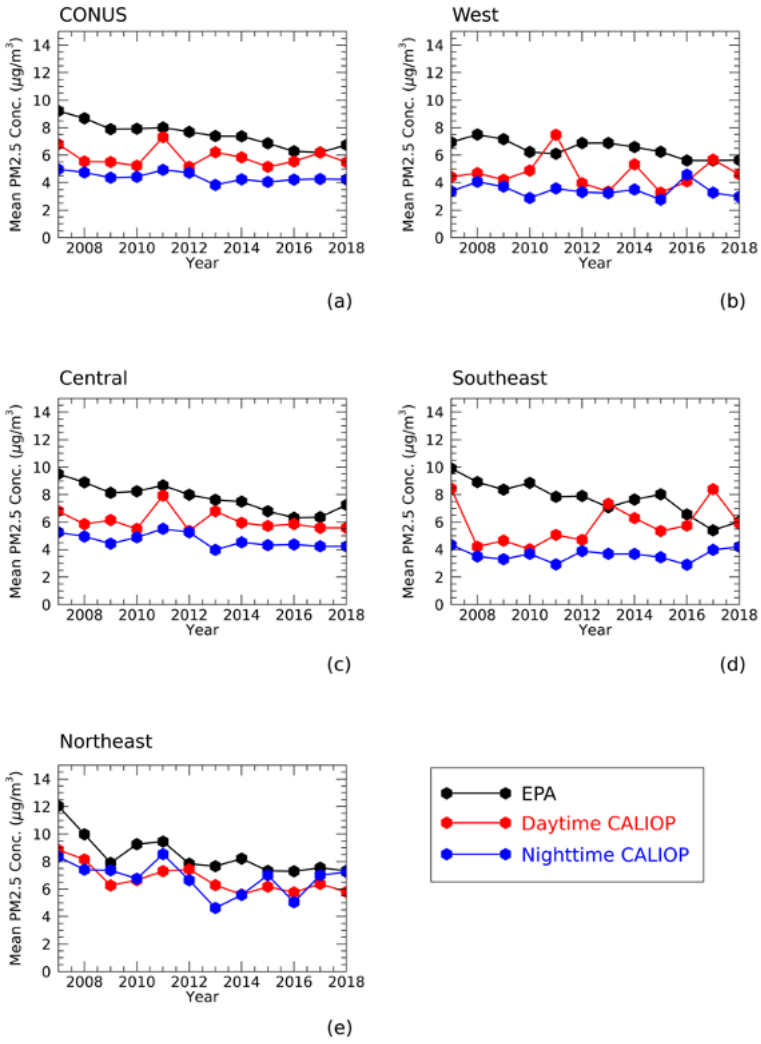

Supplemental Figure 4. Seasonal means (March through May) of $PM_{2.5}$ concentrations for each year from 2007 to 2018 at EPA stations and derived from daytime and nighttime CALIOP observations for (a) the CONUS and four regions within the CONUS: (b)West, (c) Central, (d) Southeast, and (e) Northeast.

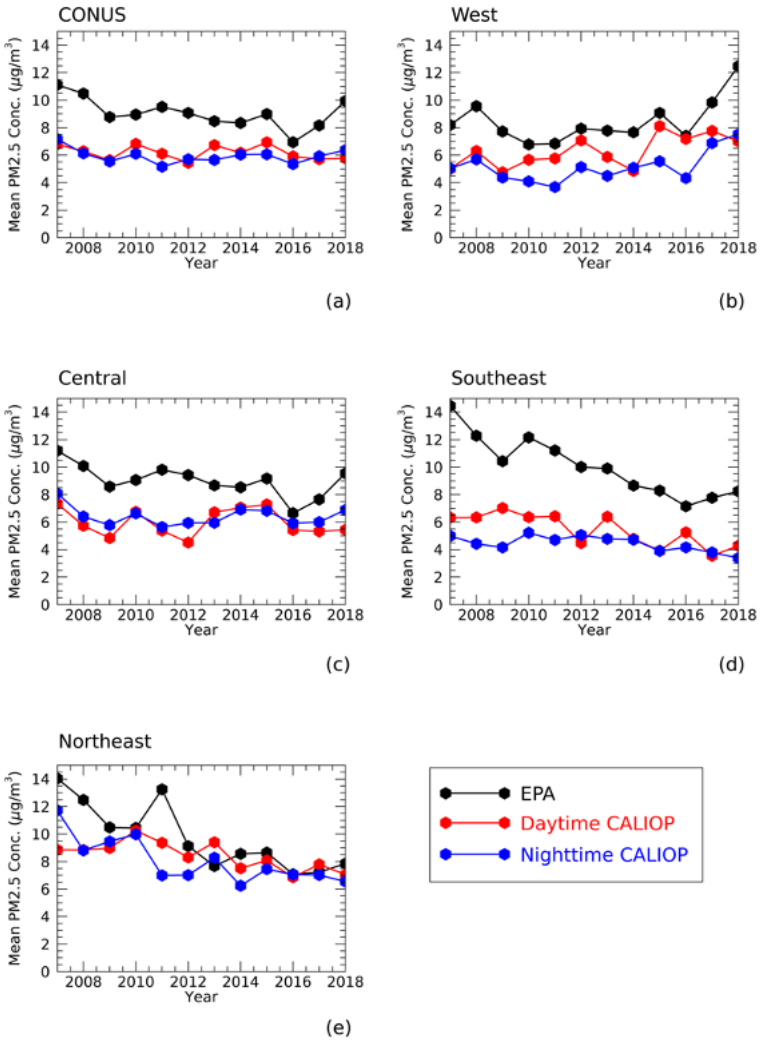

Supplemental Figure 5. Seasonal means (July through August) of $PM_{2.5}$ concentrations for each year from 2007 to 2018 at EPA stations and derived from daytime and nighttime CALIOP observations for (a) the CONUS and four regions within the CONUS: (b)West, (c) Central, (d) Southeast, and € Northeast.

1171

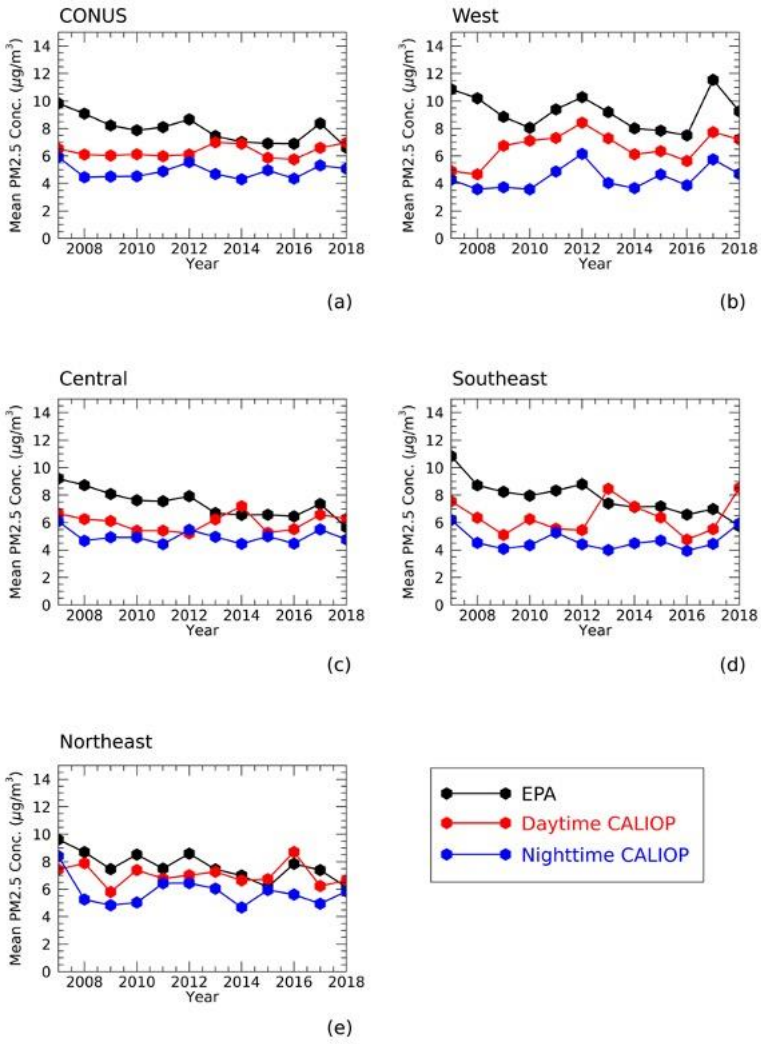

Supplemental Figure 6. Seasonal means (September through November) of $PM_{2.5}$ concentrations for each year from 2007 to 2018 at EPA stations and derived from daytime and nighttime CALIOP observations for (a) the CONUS and four regions within the CONUS: (b)West, (c) Central, (d) Southeast, and (e) Northeast.

1172
1173

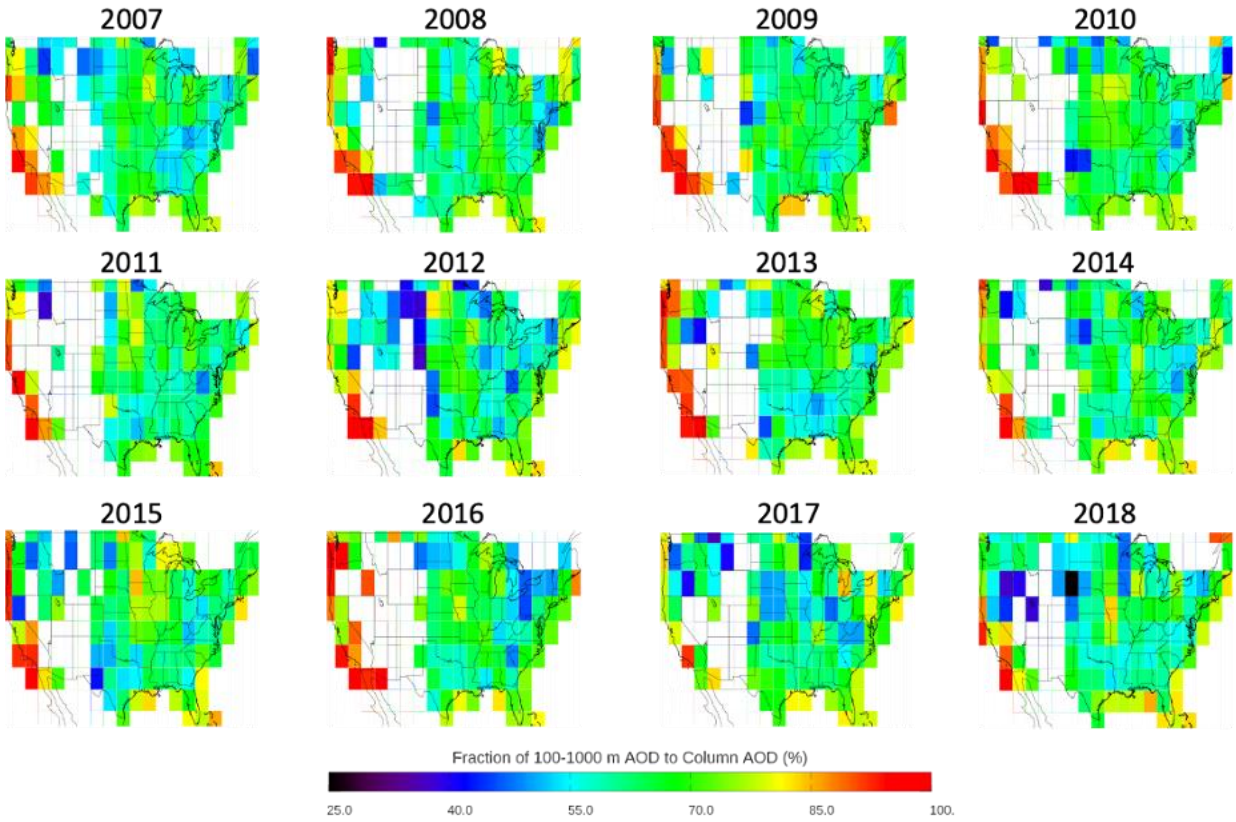

Supplemental Figure 7. For 2007 to 2018 over the CONUS, 3º x 3º yearly mean fraction of 100-1000 m AOD to column AOD (%) as observed by CALIOP during dust-free daytime conditions.

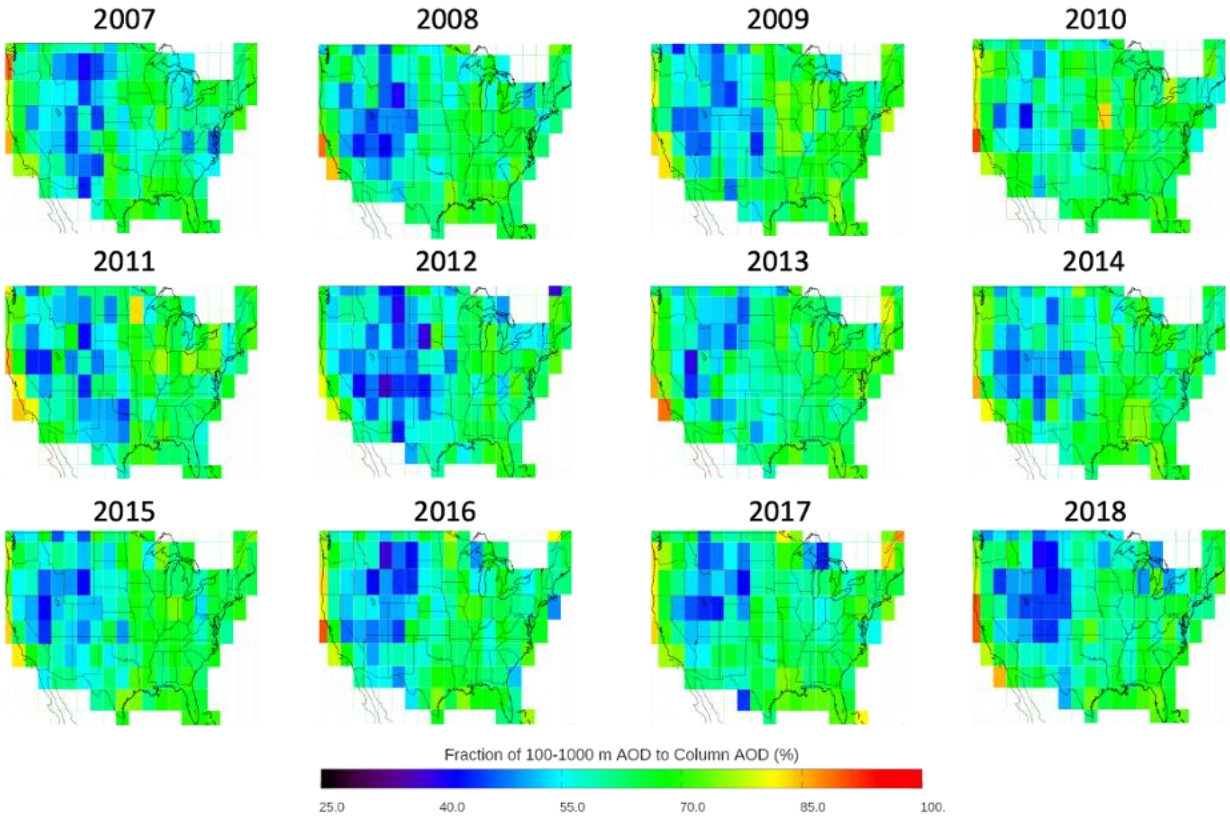

Supplemental Figure 8. For 2007 to 2018 over the CONUS, 3º x 3º yearly mean fraction of 100-1000 m AOD to column AOD (%) as observed by CALIOP during dust-free nighttime conditions.

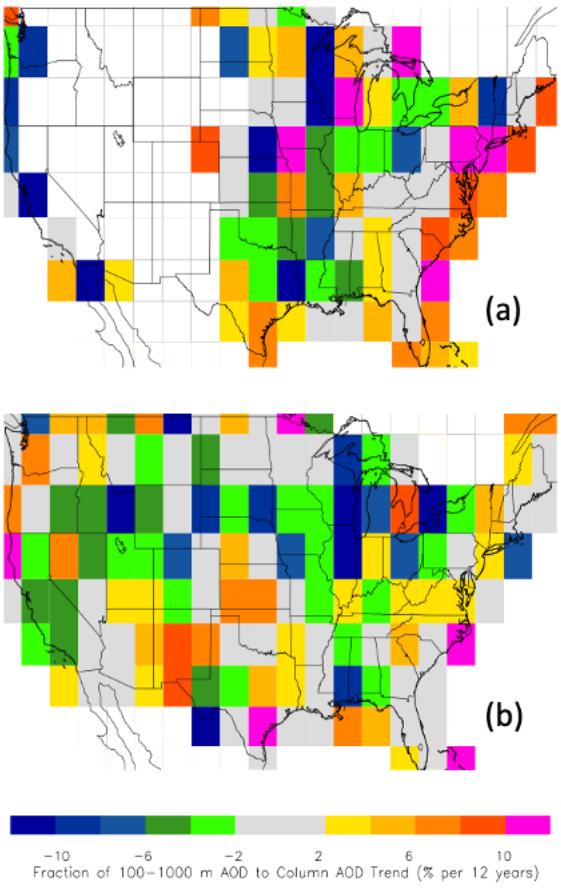

Supplemental Figure 9. Twelve-year (2007-2018) trends of fraction of 100-1000 m AOD to column AOD (% per twelve years) on a 3º x 3º grid using (a) daytime and (b) nighttime dust-free CALIOP data.